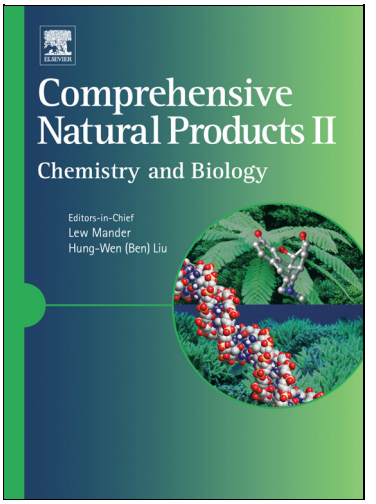

Michelle P. Roettger, Marina Bakhtina, Sandeep Kumar, and Ming-Daw Tsai.
In *Comprehensive Natural Products II Chemistry and Biology*;
Mander, L., Lui, H.-W., Eds.; Elsevier: Oxford, 2010;
volume 8, pp. 349–383.

8.10 Catalytic Mechanism of DNA Polymerases

Michelle P. Roettger, Marina Bakhtina, and Sandeep Kumar, The Ohio State University, Columbus, OH, USA

Ming-Daw Tsai, Academia Sinica, Taipei, Taiwan

8.10.1 Introduction

8.10.1.1 Basic Polymerase Function

DNA-dependent DNA polymerases are responsible for directing the synthesis of new DNA from deoxyribonucleotide triphosphates (dNTPs) opposite an existing DNA template, which contains the genetic information critical to an organism's survival. To properly preserve this information, during each round of catalysis, a polymerase must accurately select and catalyze the insertion of a complementary nucleotide (dNTP) substrate, from a pool of four structurally similar molecules, into a nascent DNA strand. Present across all three domains of life, including Archaea, Bacteria, and Eukaryota, polymerases are necessarily and diversely utilized during DNA replication, recombination, repair, and translesion synthesis (TLS).

8.10.1.2 Polymerase Fidelity and Relationship to Biological Function

To date, there are at least 15 identified human DNA polymerases possessing a myriad of functions (for reviews see Shcherbakova *et al.*,[1] Hubscher *et al.*,[2] Pavlov *et al.*,[3] and McCulloch and Kunkel[4]). These polymerases possess fidelities broadly ranging from 10^1 to 10^6, plus an additional fidelity enhancement of 10^1–10^2 when intrinsic exonuclease proofreading function is considered. Fidelity, or base substitution error, can be qualitatively regarded as a measure of the frequency by which a polymerase incorporates a correct nucleotide versus an incorrect nucleotide. A replicative polymerase replicates nondamaged DNA, and functionally requires high fidelity in order to accurately preserve genetic information, as well as to prevent mutations that may promote human diseases such as cancer.[5,6] Repair polymerases also possess a moderately high fidelity. The more recently discovered low fidelity polymerases are also of importance to human survival, as a number of them possess the capacity to bypass replication stalling lesions during replication of damaged DNA, and some may play a large role in developing the DNA sequence diversity required to effect proper immune response.

8.10.1.3 Objective

Studies examining the energetics of base pairing in solution have estimated the free energy difference between correct and incorrect base pairing to be 1–3 kcal mol^{-1}.[7,8] This translates into a fidelity of 10^1–10^2 if a polymerase were to offer no selective preference during nucleotide incorporation catalysis.[9] Clearly, the observation of higher fidelity owned by the majority of polymerases indicates that these enzymes possess a unique ability to provide significant selectivity enhancement during catalysis. Based upon the differences in free energy for correct and incorrect base pairing in solution,[8] Pol β's moderate fidelity of 10^4–10^5 translates into a selectivity enhancement of 10^2–10^3 in Pol β's active site.[10,11] After decades of research, the question remains: what is the nature of the mechanism by which such selectivity is amplified in the active site of a polymerase? This work aims to examine the catalytic mechanism of DNA polymerases, with a large focus on DNA polymerase β (Pol β) as a model system. The chapter encompasses the contributions of structural, kinetic, and computational studies in the advancement of our understanding of this mechanism. When appropriate, meaningful contributions from studies on other polymerases are discussed for comparison purposes. Some issues pertinent to the overall subject of polymerase fidelity, which include base–base hydrogen bonding, water exclusion from the active site, geometric selection, mismatch extension, exonuclease proofreading, and substrate misalignment, are briefly addressed here and we refer readers to a comprehensive review of these topics in Kunkel[12] and Kunkel and Bebenek,[13] and references therein.

8.10.2 Polymerase Families

The discovery of the first DNA polymerase, *E. coli* DNA polymerase I, by Kornberg and co-workers occurred over 50 years ago.[14,15] After extensive research spanning multiple decades, there are currently seven families of polymerases (A, B, C, D, X, Y, and RT) which are classified according to primary sequence homology and structural similarity.[16–19] Eukaryotic polymerases belong to four of these families (A, B, X, and Y) (reviewed in Shcherbakova *et al.*,[1] Hubscher *et al.*,[2] Pavlov *et al.*,[3] and McCulloch and Kunkel[4]). Defects in proper regulation

or expression of the genes encoding many of these polymerases are directly linked to phenotypic manifestation of human diseases (reviewed in Sweasy *et al.*[20]).

8.10.2.1 Family A

Belonging to Family A are *Escherichia coli* DNA polymerase I (Pol I), and eukaryotic DNA polymerases, Pol γ, Pol θ, and Pol ν. *E. coli* Pol I, the prototypical member of this family, possesses both $3' \rightarrow 5'$ and $5' \rightarrow 3'$ exonuclease activity and participates in nucleotide excision repair (NER) and Okazaki fragment processing.[21,22] The high fidelity Pol γ is the mitochondrial replicase and repair polymerase (for recent reviews see Kaguni[23] and Graziewicz *et al.*[24]). Recombinant expression of the large Pol γ subunit reveals both $3' \rightarrow 5'$ exonuclease activity and $5'$ deoxyribosephosphate (dRP) lyase activity.[25,26] The roles of the more recently discovered Pol θ and Pol ν are less clear, though both demonstrate TLS capabilities.[27–31] Pol θ has lately been implicated in the somatic hypermutation (SHM) of immunoglobulin (Ig) genes.[32–34] Among other members of this family is bacteriophage replicative DNA polymerase T7.

8.10.2.2 Family B

Notable members comprising the Family B polymerases include the prototypical *E. coli* Pol II, as well as eukaryotic polymerases, Pol α, Pol δ, Pol ε, and Pol ζ. In humans, the coordinated efforts of Pol α, Pol δ, and Pol ε are responsible for leading and lagging strand synthesis during nuclear chromosomal replication prior to cell division (for review see Pospiech and Syvaoja,[35] Hindges and Hubscher,[36] and Lehman and Kaguni[37]). During this process, Pol α acts as a primase, generating short tracts of hybrid RNA/DNA primers, which are subsequently elongated by Pol δ and Pol ε (for review see Johnson and O'Donnell[38]). Both high-fidelity Pol δ and Pol ε possess strong $3' \rightarrow 5'$ exonuclease activity, and have also been implicated in a variety of mammalian repair pathways, including NER, base excision repair (BER), mismatch repair (MMR), and double-strand break (DSB) repair. The more recently identified Pol ζ possesses proficient mismatch and lesion extension capability possibly used in conjunction with other DNA polymerases for TLS during DSB repair, interstrand cross-link repair (ICL), and SHM (recently reviewed in Lawrence[39] and Gan *et al.*[40]). Bacteriophage polymerases T4 and RB69 also belong to this family.

8.10.2.3 Families C and D

The major *E. coli* replicative polymerase Pol III belongs to Family C (for review see Kelman and O'Donnell[41] and O'Donnell *et al.*[42]). The D Family is found only in archaebacteria, and includes *Pyrococcus furiosus* (*Pfu*) Pol D.[43]

8.10.2.4 Family X

The X Family of DNA polymerases houses Pol β, the prototypical polymerase of this family. Pol β serves as a good model system for polymerase mechanism due to its small size, lack of intrinsic exonuclease activity, and stability under a variety of conditions. Studies both *in vivo* and *in vitro* have unequivocally demonstrated Pol β's important role in single-nucleotide gap filling during the short-patch mammalian BER process.[25,44–46] This pathway is modeled as follows (for review see Parikh *et al.*,[47] Wilson,[48] and Lindahl and Wood[49]). A DNA glycosylase creates an apurinic/apyridinic (AP) site through removal of a damaged base in duplex DNA through breakage of the *N*-glycosidic bond. An AP endonuclease then cleaves the phosphodiester backbone $5'$ to the sugar, thus generating a $3'$-hydroxyl group and a dRP flap. Pol β then fills the gap with an undamaged nucleotide, and afterward Pol β's 8-kDa lyase domain is responsible for the removal of the dRP through a β-elimination mechanism.[50] Finally, the nicked duplex DNA is sealed by either DNA ligase I or DNA ligase III.[51,52]

Other members of this family include eukaryotic terminal deoxynucleotidyl transferase (TdT), Pol μ, Pol λ, and Pol σ. TdT is known to function in antigen receptor diversification during V(D)J recombination through addition of nucleotides (N additions) to gene segment junctions in a template-independent manner[53–55] (reviewed in Fowler and Suo[56]). The more recently discovered Pol λ and Pol μ have been implicated in

general DSB repair, but the specific context of their roles remains to be established (for review see Nick *et al.*[57] and Moon *et al.*[58]). Pol σ is involved in the establishment of sister chromatid cohesion.[59,60] The African swine fever virus (ASFV) Pol X also belongs to this family. ASFV Pol X is the smallest of all known polymerases, and plays a gap-filling role during BER of viral DNA.[61]

8.10.2.5 Family Y

Members of the newly discovered low-fidelity Y Family are exonuclease deficient, possess TLS abilities, and include eukaryotic Pol η, Pol ι, Pol κ, and REV1, and *Sulfolobus solfataricus* DNA polymerase IV (Dpo4). Pol η, Pol ι, and Pol κ have all been shown to interact with the deoxycytidyltransferase, REV1, which may act as a scaffold during polymerase switching, the process by which the aforementioned TLS polymerases are coordinated in their projected participation in either DSB repair (Pol η), BER (Pol ι), NER (Pol κ), and SHM (Pol η and Pol ι) (reviewed in Rattray and Strathern,[62] Prakash *et al.*,[63] Lehmann *et al.*,[64] Lehmann,[65,66] Kannouche and Lehmann,[67] Prakash and Prakash,[68] Kunkel *et al.*,[69] and Vaisman *et al.*[70]).

8.10.2.6 Family RT

HIV-1 reverse transcriptase (RT) possesses DNA and RNA template-dependent polymerase activity, as well as an endonucleolytic ribonuclease H (RNase H) activity responsible for degradation of the RNA in an RNA/DNA duplex. Because RT plays a critical role in the HIV life cycle, it remains a primary therapeutic target for anti-HIV drug development.[71–73]

8.10.3 Structural Requirements for Polymerase Catalysis

8.10.3.1 General Domain/Subdomain Architecture of DNA Polymerases

Although all DNA polymerases do not share significant primary sequence homology, they do share several architectural features in common. Pol β topology consists of two domains: an N-terminal 8-kDa lyase domain and a C-terminal 31-kDa polymerase domain. The N-terminal domain binds the 5′-phosphate of the downstream primer in short gapped DNA substrates,[74] and possesses dRP lyase activity that proves essential for successful completion of BER.[75,76] Upon functional alignment, the C-terminal domain of Pol β,[77,78] possessing DNA polymerization capability, resembles the overall structure of other polymerases, such as HIV-1 reverse transcriptase,[79] bacteriophage T7 DNA polymerase,[80] and Klenow fragment (KF) of *E. coli* DNA polymerase I,[81] in maintaining the canonical polymerase architecture which resembles a hand and consists of fingers, palm, and thumb subdomains, according to the nomenclature suggested by Steitz *et al.*[82] The fingers, palm, and thumb subdomains of all polymerases functionally correspond to actions of nascent base pair binding (N-subdomain), catalysis (C-subdomain), and double-strand DNA binding (D-subdomain), respectively (**Figure 1**). In this chapter, we use this functionally based nomenclature[83] to describe subdomain motions. The spatial orientation of three conserved acidic amino acid residues in the C-subdomain which coordinate the two metal ions required for catalysis (Section 8.10.3.3) are superimposable among polymerase families. Members of the Y-family of DNA polymerases possesses an additional little finger subdomain, or polymerase-associated domain (PAD), which assists in DNA binding.[84]

8.10.3.2 Polymerases Undergo a Global Conformational Change upon dNTP Binding

Multiple crystal structures of polymerases solved in unliganded and various liganded states are of significant importance to polymerase mechanism studies. For example, the plethora of available structures for Pol β include: free enzyme,[85,86] binary complexes of enzyme with gapped, nicked, or blunt-ended DNA,[78,87] and ternary complexes of enzyme, DNA, and correct incoming dNTP.[78,86,88–90] Comparison of Pol β's binary gapped DNA complex with the ternary gapped DNA complex containing correct incoming nucleotide ddCTP, reveals that there is a dNTP-induced subdomain closure originating from the N-subdomain in which there is a 30° rotation of α-helix N toward the nascent base pair along the hinge axis of α-helix M.[78] This movement of

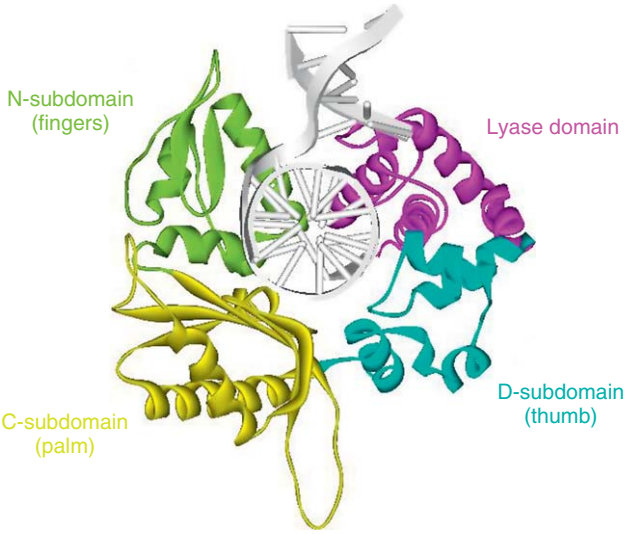

Figure 1 Subdomain organization of Pol β (from ternary complex structure 1BPY as reported in M. R. Sawaya; R. Prasad; S. H. Wilson; J. Kraut; H. Pelletier, *Biochemistry* **1997**, *36*, 11205–11215.[78]) The C-terminal polymerase domain is subdivided into three subdomains: DNA binding D-subdomain (cyan), catalytic C-subdomain (gold), and nascent base pair binding N-subdomain (green). The N-terminal lyase domain is highlighted in pink. DNA is shown in gray.

α-helix N by Pol β, paralleled by movement of α-helix O in T7 and Klentaq[80,91] and β3–β4 in HIV-1 RT,[79] serves to create a tight binding pocket for the nascent base pair, bringing about important interactions between polymerase side chains and the minor groove edge of DNA, as well as with the base, sugar, and triphosphate of the incoming dNTP (**Figure 2**).

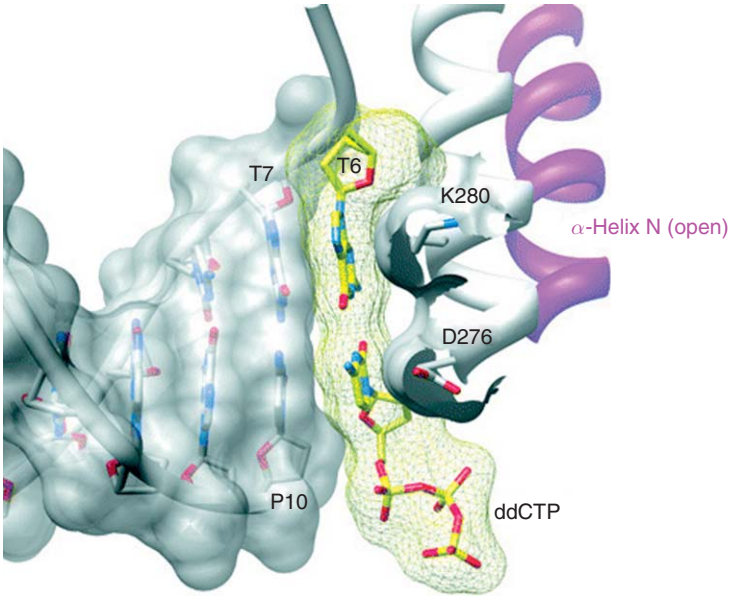

Figure 2 Positioning of α-helix N upon Pol β N-subdomain closure. Pictured are the nascent base pair (incoming and templating nucleotides) (yellow), the semitransparent molecular surface of the upstream DNA duplex (gray), and the molecular surface of the nascent base pair (yellow mesh). In the closed conformation (white), Asp276 and Lys280 of α-helix N stack with the bases of the incoming and templating nucleotides, respectively. These interactions are lost in the open conformation (magenta). Reproduced from W. A. Beard; S. H. Wilson, *Chem. Rev.* **2006**, *106*, 361–382. Copyright 2006 American Chemical Society.

Overall, the crystal structures of many polymerases to date, including Pol β, yield important mechanistic insights in implicating the existence of a large conformational change that occurs upon correct nucleotide binding, from an 'open' E•DNA binary complex conformation to a 'closed' E′•DNA•dNTP ternary complex conformation (for review see Sawaya *et al.*,[78] Doublie *et al.*[80] and Beard and Wilson[83]). Formation of the 'closed' ternary complex is a prerequisite to chemistry in order to provide proper active-site alignment. Existence of this conformational change has led to the proposal of a general 'induced-fit' mechanism,[92] in which this conformational change is postulated to be the major contributor to polymerase fidelity.[13,93]

There appears to be a correlation of polymerase fidelity with active-site spaciousness.[94] Crystal structures of low-fidelity Y-family DNA polymerases differ from higher fidelity polymerases in possessing distinctly smaller N- and D-subdomains, which give rise to a largely solvent-accessible active site. This structural feature allows for flexibility in accommodation of bulky lesions (for review see Prakash *et al.*[63]). Furthermore, it appears that some of the Y-family members do not undergo an open-to-closed conformational transition upon dNTP binding, as evidenced by comparison of the binary and ternary complexes of Dpo4[95–97] and Pol ι.[98]

8.10.3.3 Two Metal-Ion Mechanism

Pol β utilizes a 'two metal-ion' mechanism for nucleotide incorporation chemistry.[99] This mechanism is likely conserved for all DNA and RNA polymerases.[82,100] Crystal structures of Pol β ternary complexes were the first to validate this mechanism on a structural basis.[78,86] Three highly conserved catalytic residues of C-subdomain, Asp 190, Asp192, and Asp256, coordinate two metal ions (**Figure 3**). Metal ion A coordinates dNTP in a tridentate fashion, and presumably enters the active site as a Mg•dNTP complex. Metal ion B coordinates the 3′-oxygen of the primer, as well as the pro-R_p oxygen of the α-phosphate of the incoming nucleotide, and is referred to as the catalytic Mg^{2+} ion in mechanism studies. Both hexacoordinated metal ions serve to stabilize the structure and charge of the pentacovalent transition state formed upon in-line nucleophilic attack of the α-phosphate of an incoming nucleotide by the primer's 3′-oxygen. The nucleotidyl transfer reaction continues through the transition state as the primer increases one nucleotide in length and a pyrophosphate leaving group is formed (**Figure 3**).

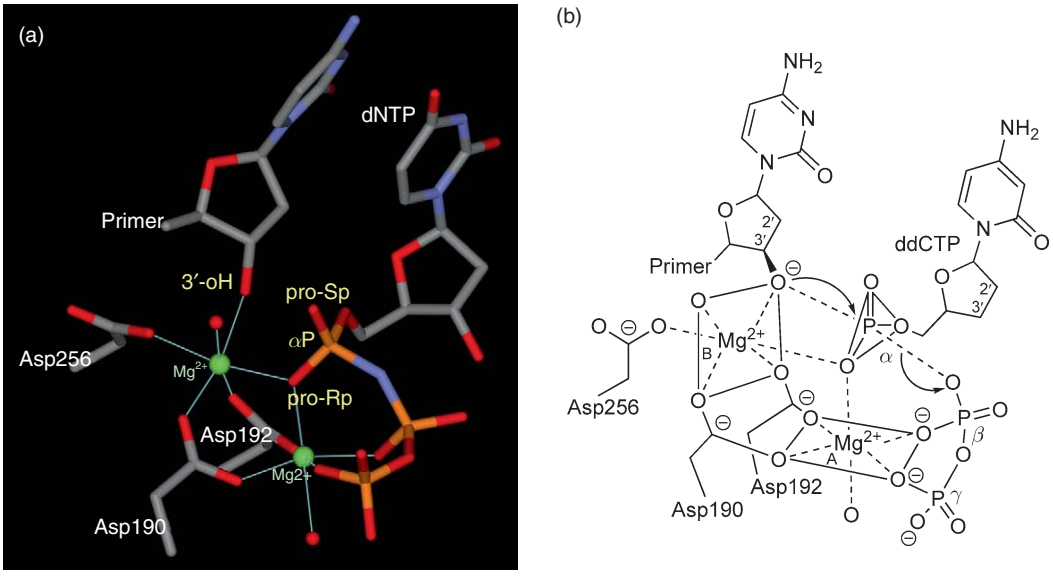

Figure 3 Nucleotidyl transfer mechanism of Pol β. (a) Orientation of incoming dNTP in the DNA Pol β active site depicted from the ternary complex structure 2FMS as reported in V. K. Batra; W. A. Beard; D. D. Shock; J. M. Krahn; L. C. Pedersen; S. H. Wilson, *Structure* **2006**, *14*, 757–766. Pro-S_p and pro-R_p oxygens on the α-phosphate of the incoming dNTP moiety are labeled. Magnesium ions are shown in green. The catalytic Mg^{2+} interacts with pro-R_p non-bridging oxygen. (b) Schematic representation of nucleophilic attack to form a pentacovalent transition state as modeled from ternary complex structure 1BPY. Part B is reproduced with permission from M. R. Sawaya; R. Prasad; S. H. Wilson; J. Kraut; H. Pelletier, *Biochemistry* **1997**, *36*, 11205–11215. Copyright 1997 American Chemical Society.

8.10.4 General Mechanism of Nucleotide Incorporation Catalyzed by DNA Polymerases

8.10.4.1 Modern Methods Used in DNA Polymerase Mechanism Studies

Consistent with their important roles in living organisms, DNA polymerases are objects of intensive multifaceted studies employing a broad spectrum of biochemical and biophysical methods in conjunction with cellular and molecular biology approaches. In-depth studies of DNA polymerase mechanism require application of modern biophysical techniques and a variety of molecular probes. Great advances in our understanding of the mechanism of dNTP incorporation can be attributed to the utilization of a variety of modern approaches including rapid mixing techniques (rapid chemical quench and stopped-flow), FRET-based kinetics, fluorescence-based assays, and single molecule kinetics. These techniques allow us to monitor the overall progress of single-nucleotide incorporation, as well as to probe specific steps along the reaction pathway, for example, by varying reaction conditions, applying substrate analogues, or altering an enzyme active site through site-directed mutagenesis. This section begins with an overview of the principal methods used in mechanistic studies of DNA polymerases and the main conclusions obtained in these studies. Then we focus on a detailed characterization of DNA polymerase kinetic mechanism using Pol β as a model enzyme. Note that the main purpose of this chapter is to examine the mechanism of dNTP incorporation, therefore it does not include many other important aspects of DNA polymerase function such as DNA substrate recognition and binding, processivity, and self-editing mechanisms.

8.10.4.1.1 Pre-steady-state kinetics using discontinuous assays (rapid chemical quench)

Pre-steady-state (or transient-state) kinetic approaches, allowing the dissection of individual steps and intermediates in an enzymatic reaction, are superior to classical steady-state approaches. Pre-steady-state kinetic methods were first applied to DNA polymerases in late 1980s to early 1990s in classical studies of *E. coli* Pol I (Klenow fragment, KF)[101–104] and bacteriophage T7 DNA polymerase.[105,106] These studies have served as a framework for the kinetic analysis of many polymerases to date. The general polymerase kinetic mechanism derived from these studies and subsequent studies of Pol β is presented in **Figure 4**.

Under pre-steady-state conditions, the enzyme in the reaction is used in stoichiometric amounts, meaning that one of the substrates has a concentration smaller than or comparable to the enzyme concentration. In single-turnover DNA polymerase assays of dNTP incorporation, the enzyme concentration is in excess of the DNA substrate concentration. These conditions allow us to follow the enzyme through one complete catalytic cycle, thus eliminating complications from multiple turnovers. Nucleotide incorporation is a relatively fast process occurring on a millisecond timescale, and rapid chemical quench is the specialized instrument generally

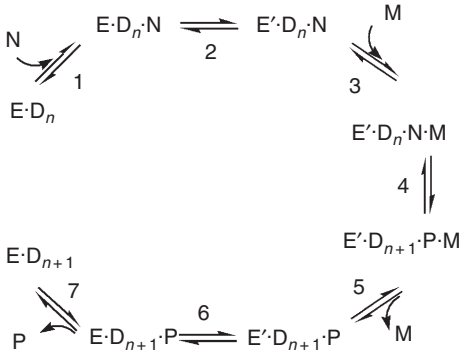

Figure 4 Simplified kinetic scheme of single-nucleotide incorporation by a DNA polymerase. Step 1, Mg•dNTP binding; step 2, N-subdomain closing; step 3, catalytic Mg^{2+} binding; step 4, nucleotidyl transfer (chemistry); step 5, catalytic Mg^{2+} dissociation; step 6, N-subdomain reopening; step 7, pyrophosphate release. E = DNA polymerase in open conformation; E′ = closed conformation; D_n = DNA substrate; D_{n+1} = DNA product elongated by addition of one nucleotide; N = Mg•dNTP; M = catalytic Mg^{2+}; P = Mg•PP_i. Reproduced with permission from M. Bakhtina; S. Lee; Y. Wang; C. Dunlap; B. Lamarche; M. D. Tsai, *Biochemistry* **2005**, *44*, 5177–5187. Copyright 2005 American Chemical Society.

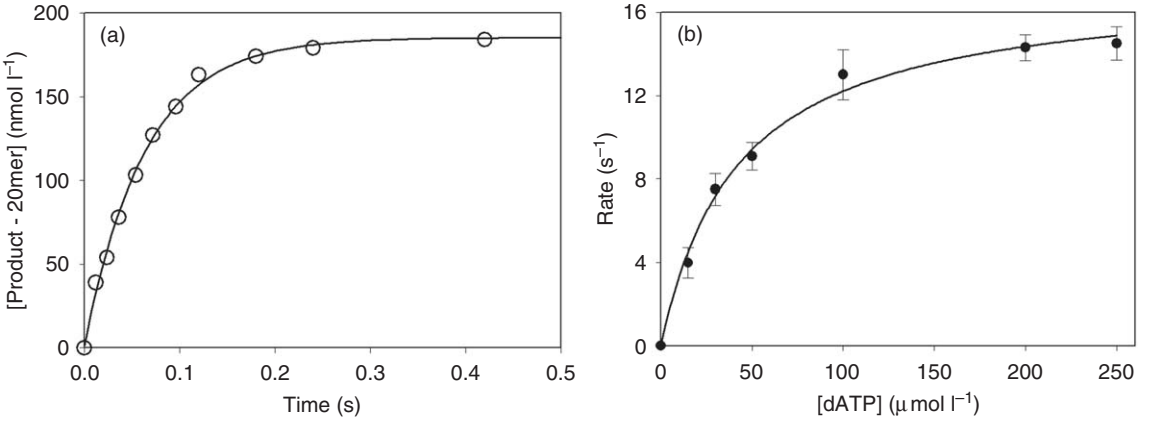

Figure 5 Typical rapid chemical quench assay of single-nucleotide incorporation by Pol β. (a) Single-turnover time course of DNA product formation fitted to a single exponential equation $[DNA_{n+1}] = A(1-e^{-k_{obs}t})$. (b) Plot of rate versus dATP concentration fitted to a hyperbolic equation $k_{obs} = k_{pol}[dNTP]/(K_{d,app} + [dNTP])$ to obtain values for $K_{d,app}$ and k_{pol}. Adapted with permission from C. A. Dunlap; M. D. Tsai, *Biochemistry* **2002**, *41*, 11226–11235. Copyright 2002 American Chemical Society.

employed to obtain time courses for single-nucleotide incorporation into a DNA substrate. The primer strand of duplex DNA usually carries a ^{32}P-labeled phosphate group or a fluorescent label, so the initial DNA substrate (D_n, where n is the length of the primer) and DNA product (D_{n+1}, where primer is extended in length by one nucleotide) can be resolved and quantified. The observed first-order rate constant of DNA product formation can be obtained from single exponential fit of a plot of the concentration of extended primer versus time (**Figure 5(a)**). Two important kinetic constants, $K_{d,app}$ (the apparent constant of nucleotide dissociation from kinetically active ternary complex) and k_{pol} (the maximum rate constant of single dNTP incorporation), can be obtained from a hyperbolic dependence of the observed rate constant on nucleotide concentration (**Figure 5(b)**). Another important parameter is the ratio of $k_{pol}/K_{d,app}$, which defines the 'catalytic efficiency' constant. The comparison of $k_{pol}/K_{d,app}$ values for correct and incorrect dNTP incorporation serves as a quantitative measure of DNA polymerase fidelity. Fidelity is defined as $[(k_{pol}/K_{d,app})_{cor} + (k_{pol}/K_{d,app})_{inc}]/[(k_{pol}/K_{d,app})_{inc}]$ – where the subscripts 'cor' and 'inc' indicate correct (matched) and incorrect (mismatched) nucleotide incorporation, respectively. In general, fidelity analysis of multiple polymerases reveals that the catalytic efficiencies for matched dNTP incorporation vary widely, whereas the catalytic efficiency for mismatched dNTP incorporation is relatively constant.[107,108]

The interpretation of kinetic parameters in terms of microscopic steps in the reaction pathway depends on the kinetic mechanism of the enzyme. For example, $K_{d,app}$ is often misinterpreted as the thermodynamic dNTP dissociation constant. This would be true if a rapid-equilibrium dNTP binding (step 1 in **Figure 4**) was directly followed by the rate-limiting and virtually irreversible step (this would be step 2 in **Figure 4**). However, as shown later, numerous evidences argue against this scenario, instead pointing to the existence of a fast conformational step (or even multiple steps) prior to the rate-limiting step. It is also important to mention that pre-steady-state kinetic experiments are generally designed with the assumption that DNA polymerases initially form a binary complex with a DNA substrate and then bind a nucleotide substrate. Earlier studies of the kinetic order of substrate binding have concluded that DNA polymerases possess a sequential ordered mechanism where DNA binding always occurs before productive dNTP binding.[109–111] This proposed mechanism is consistent with the template-directed and processive nature of nucleotide incorporation catalyzed by 'classical' high-fidelity DNA polymerases. However, a number of recently discovered DNA polymerases with novel properties,[112] possessing low fidelity, selectivity for certain base pairs, and the ability to use damaged/unnatural substrates, might not necessarily follow the same substrate binding order. For instance, one of the lowest fidelity polymerases, ASFV Pol X, possesses an altered order of substrate binding, with dNTP as the preferred first substrate.[113]

Information extracted from kinetic data collected under 'burst' conditions, in which there is a two- to fourfold excess of DNA substrate over DNA polymerase, illustrates another important application of pre-steady-state experiments. This type of experiment provides useful information about the transient concentration of kinetically active ternary complex. A time course of DNA product formation under these conditions demonstrates a transient exponential phase followed by a steady-state linear phase. By examining the dependence of the burst amplitude on DNA concentration, the enzyme's binding affinity for DNA can be evaluated.

'Burst' conditions have historically been utilized in the pulse-chase/pulse-quench experiment. In the pulse-quench portion of the experiment, a strong acid is used as a chemical quencher of the dNTP incorporation reaction, immediately quenching all enzyme species. In the pulse-chase portion of the experiment, addition of a large excess of nonlabeled dNTP allows incorporation of radiolabeled dNTP trapped in the DNA polymerase active site (**Figure 6**). In KF studies,[101] observation of 20% larger 'burst' amplitude in the pulse-chase compared to the pulse-quench indicates the accumulation of kinetically active E•DNA•dNTP ternary complex in a 'closed' conformation (i.e., in a conformation where dNTP bound in the active site cannot be exchanged with dNTP in solution). Note that the kinetic evidence of the existence of the 'closed' E•DNA•dNTP conformation (which in turn suggests the existence of an 'open-to-closed' conformational change) was obtained before X-ray structural evidence.

It is necessary to mention that the results of pulse-chase/pulse-quench experiments are often interpreted as an evidence for the existence of a rate-limiting conformational step. However, while indicating the existence of a conformational step before the nucleotidyl transfer step (chemistry), the results do not prove that this conformational step is rate limiting. Moreover, observation of transient appearance of the 'closed' conformation would not be possible if the conformational step was much slower than other microscopic steps in the reaction

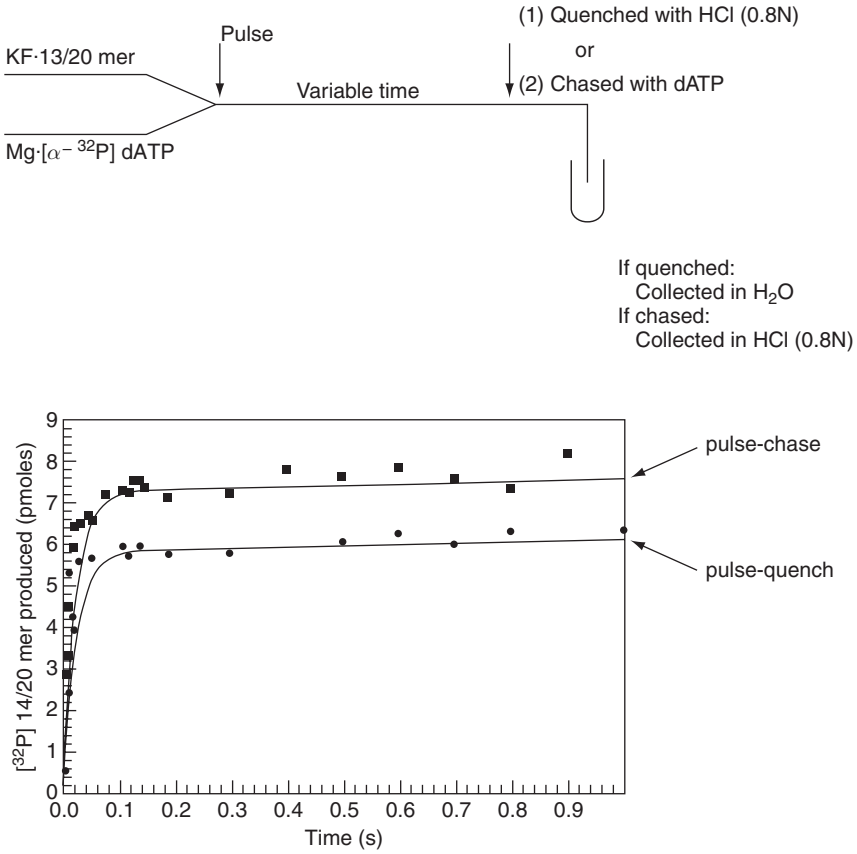

Figure 6 Pulse-chase/pulse-quench experimental design and results obtained for KF. Reproduced with permission from M. E. Dahlberg; S. J. Benkovic, *Biochemistry* **1991**, *30*, 4835–4843. Copyright 1991 American Chemical Society.

pathway. Indeed, there are two conditions that need to be satisfied for the larger 'burst' amplitude to be observed in the pulse-chase compared to the pulse-quench experiment:

1. The rate of the reverse step (k_{-2} in **Figure 4**) cannot be much faster than the rate of forward chemistry step (k_4 in **Figure 4**), so that the majority of the 'closed' ternary complex forms the product.
2. The rate of forward reaction (k_4 in **Figure 4**) cannot be much faster than the rate of 'closing' (k_2 in **Figure 4**), so that an appreciable amount of the 'closed' ternary complex is accumulated.

Pulse-chase/pulse-quench experiments with KF[101] indicated accumulation of the nucleotide bound enzyme species, which would not be possible if the forward reaction was much faster than the rate of conformational 'closing.' To explain this observation, the authors proposed the presence of a kinetic 'road block' – a slow step after the phosphodiester bond formation. However, the results of the pulse-chase/pulse-quench experiments can also be explained by designating chemistry as the slow step, meaning that the chemical step itself plays the role of the 'road block.' The conclusion that chemistry is a fast step in the KF reaction pathway was made based on the observation of a small thio-effect magnitude,[104] which, as elaborated in the following section, should not be used as a solid evidence of the chemical step being nonrate limiting.

8.10.4.1.2 Use of substrate analogues to probe DNA polymerase mechanism

1. *Use of phosphorothioate dNTP analogues.* Nucleotide analogues, in which the nonbridging oxygen at the α-phosphate (αP) is substituted with a sulfur atom, can be used to probe active-site environment. Such substitution makes αP a chiral center, resulting in S_p and R_p stereoisomers of phosphorothioate dNTP analogues. As is the case for many other enzymes which catalyze phosphoryl transfers, DNA polymerases demonstrate stereoselectivity – specifically maintaining a preference toward incorporation of the S_p isomer (**Figure 3**). The most straightforward explanation of the observed stereoselectivity is that the magnesium ion essential for catalysis preferably binds an oxygen ('hard' ligand). If this were the major reason for the observed stereoselectivity, substitution of a 'hard' Mg^{2+} for a 'softer' metal would be expected to reverse the observed stereoselectivity such that the R_p isomer would be preferred. Contrary to that predicted, results of Pol β and KF studies by Burgers and Eckstein[114] and Liu and Tsai[115] have demonstrated that the polymerases select S_p-dNTPαS even in the presence of a 'soft' Mn^{2+}, Cd^{2+}, or Co^{2+} ligand, though with slightly lower selectivity. In light of these results, it is likely that other factors, possibly involving the active-site geometry, play determining roles in selection of the S_p-dNTPαS analogue.

   Thio-substituted dNTP analogues were widely used in early studies of DNA polymerases to address the question of whether or not phosphodiester bond formation is the rate-limiting step in the nucleotide incorporation pathway. The thio-effect is defined as the ratio of phosphoryl transfer rates for a nonsubstituted nucleotide substrate and its corresponding thio-analogue ($k_{pol,dNTP}/k_{pol,dNTP\alpha S}$). Owing to its decreased electronegativity, sulfur is less effective in withdrawing electron density from the central phosphorus atom, making the α-phosphorus less accessible to nucleophilic attack by 3′-OH group of DNA primer terminus. Based on model nonenzymatic reactions of phosphorothioate diesters, the expected range for the thio-effect is 4–11.[116] Application of thio-analogues in DNA polymerase studies revealed that a number of polymerases demonstrate only a three- to fourfold slower rate for sulfur-substituted nucleotide analogue incorporation.[104,105,117] The absence of a full magnitude of thio-effect was interpreted as evidence that chemistry is not the rate-limiting step in the DNA polymerase catalyzed nucleotide incorporation pathway. However, the enzyme active-site environment could potentially affect the magnitude of the 'intrinsic thio-effect' (defined as the observed thio-effect when the chemical step is fully rate limiting), by either increasing or decreasing it. Let us consider a hypothetical nonenzymatic model that perfectly represents the DNA polymerase catalyzed reaction. In this case, the model reaction would occur in an achiral environment where both nonbridging oxygens make an equal contribution to the transition state stabilization. In contrast, the pro-R_p and pro-S_p positions are not equal within the DNA polymerase active site, such that the divalent metal ion coordination occurs exclusively with the pro-R_p oxygen atom (**Figure 3**). This should result in a larger electron-withdrawing role for the pro-R_p oxygen, and therefore a less important contribution of the pro-S_p

oxygen toward transition state stabilization. Consequently, the isomer with the pro-S_p oxygen substituted for sulfur (i.e., the S_p isomer) is expected to demonstrate a smaller reduction in dNTP incorporation rate than the R_p isomer, and since DNA polymerases accept S_p-dNTPαS analogues almost exclusively, this would result in a smaller intrinsic thio-effect than initially predicted by nonenzymatic reactions of phosphorothioate diesters.

2. *Use of halomethylene-modified β–γ bridging dNTP analogues.* A linear free energy relationship (LFER) is a powerful tool for examination of reaction mechanisms. Nucleotide analogues modified at the β–γ bridging oxygen have been used to probe the contribution of leaving group elimination to the overall rate of dNTP incorporation catalyzed by DNA polymerase β.[118,119] A variety of halomethylene-modified dNTP analogues can be used to provide a broad range of leaving group pK_as. Evaluation of LFER for the Pol β catalyzed reaction revealed a strong correlation between the logarithm of the observed rate constant and leaving group pK_a. The observed Brønsted correlation with a steep slope suggests that P–O bond breaking is at least partially rate limiting (**Figure 7**).

   The chemical transformation necessary for dNTP insertion by DNA polymerases (step 4 in **Figure 4**) can be considered as a progression of the following events: 3′ OH nucleophile activation (deprotonation), nucleophilic attack on the α-phosphate of incoming dNTP (P–O bond formation), and pyrophosphate leaving group departure (P–O bond cleavage). Evaluation of transition state free energy values associated with each of these microscopic steps is a focus of extensive quantum and molecular mechanical calculation studies, which often result in contradicting conclusions (see Section 8.10.5). Notably, results of Pol β studies using halomethylene-modified dNTP analogues, pH dependence, and the kinetic isotope (deuterium) effect suggest that all three microscopic steps make a significant contribution to the overall rate of single-nucleotide incorporation, or in other words, all three steps have comparable transition state energies.[119]

3. *Analogues with modified nucleobases.* Various dNTP analogues modified at the nucleobase have been synthesized and used to probe mechanism of DNA polymerase selectivity toward correct base pair formation.[120] Factors that probably affect the selectivity of nucleotide incorporation include base pair hydrogen bonding, steric factors such as base pair size and shape, and base stacking interactions. A generally accepted hypothesis suggests that polymerases check the geometry of base pairing through hydrogen bonds and steric interactions with the minor groove of the DNA. Steric and hydrogen bonding factors have been studied for several DNA polymerases utilizing series of systematically altered dNTP analogues.[121,122] The most striking results were obtained with difluorotoluene (F in **Figure 8**) – a nucleobase analogue that has the same shape as thymine, but lacks hydrogen bond-forming capability.

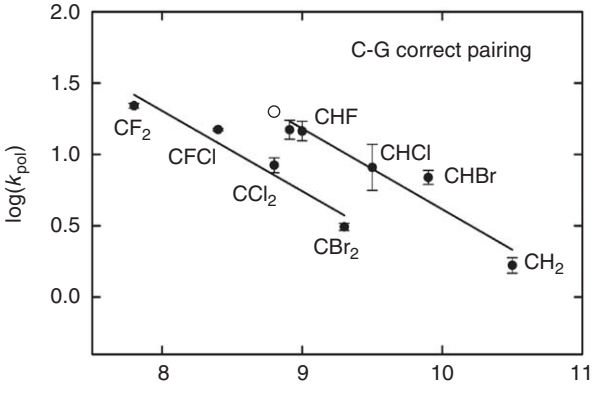

Figure 7 Brønsted correlations of log(k_{pol}) versus leaving-group pK_a. Data for correct dG:dC incorporation catalyzed by Pol β. The data for monohalogenated analogues, the methylene analogue, and native dGTP conform to a linear relationship with $\beta_{lg} = -0.56$. The catalytic sensitivity to leaving group ability in this region is similar to that reported for other enzymatic P–O bond cleavages and suggests leaving-group elimination is rate limiting (or near rate-limiting). The di-halogenated analogues (connected by a separate solid line) show deviation from the other data, suggesting the possibility of a steric effect on k_{pol}. Reproduced with permission from C. A. Sucato; T. G. Upton; B. A. Kashemirov; J. Osuna; K. Oertell; W. A. Beard; S. H. Wilson; J. Florian; A. Warshel; C. E. McKenna; M. F. Goodman, *Biochemistry* **2008**, *47*, 870–879. Copyright 2008 American Chemical Society.

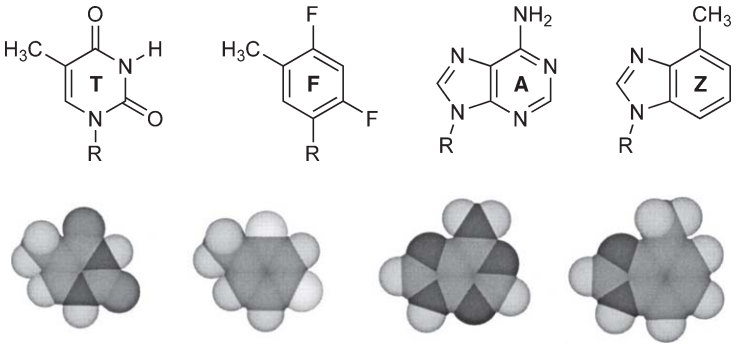

Figure 8 Structure and shape of two natural nucleosides (A and T), alongside two nonpolar analogues (Z and F). Reprinted, with permission, from the *Annual Review of Biophysics and Biomolecular Structure*, Volume 30 ©2001 by Annual Reviews www.annualreviews.org.

If hydrogen bonding makes a major contribution to nucleotide selectivity, the expected dNTP incorporation efficiency opposite templating dF would be greatly reduced. However, several studies on KF, T7, HIV-1 RT, and Taq polymerase have demonstrated that these enzymes are able to incorporate dATP opposite templating dF (forming dA:dF base pair) with efficiency and accuracy comparable to incorporation opposite templating dT.[123–125] Similar results were obtained with 4-methylbenzimidazole (Z in **Figure 8**), which closely mimics the shape of adenine. Use of dFTP and dZTP as nucleotide substrates in polymerization reactions also revealed that they can be efficiently and selectively inserted opposite templating dA and dT, correspondingly. The aforementioned results indicate that hydrogen bonding alone does not account for the origin of DNA polymerase selectivity. Steric effects were further investigated using a series of thymine analogues in which size and shape were gradually changed by use of variably sized atoms (H, F, Cl, Br, and I) to replace the oxygens.[126] Results with KF show that both replication efficiency and fidelity initially increase through the series, reaching a maximum at the chlorinated analogue. Then, as a steric limit is apparently reached, bulkier compounds demonstrate substantially decreased efficiency and selectivity. These results reinforce a tight steric fit within the polymerase active site that plays an essential role in DNA replication fidelity.

On the contrary, application of nucleotide substrate analogues lacking hydrogen bonding potential to mammalian DNA polymerases α, β, and γ suggest that hydrogen bond energy does contribute significantly to substrate selectivity for these polymerases.[126,127] Furthermore, in Pol α studies, application of an array of purine nucleotide analogues with systematically removed or added H-bond forming groups revealed importance of these groups for correct dNTP selection, while the shape of the base pair was found to be essentially irrelevant.[121] It is evident that the relative contribution of steric fit and hydrogen bonding to nucleotide selection differs among polymerases.

8.10.4.1.3 Site-directed mutagenesis and sequence alignment

Another very powerful approach to gaining additional information about the contribution of individual residues to polymerase catalysis is to introduce specific alteration of amino acid residues through site-directed mutagenesis. Sequence alignment examining homology between previously studied family members can also be used to speculate on the effect that site-directed mutagenesis of a specific residue may have on an enzyme. For example, the Tyr–Phe motif found in the α-helix M of the N-subdomain of X-family members Pol β (Tyr271–Phe272) and Pol λ (Tyr505–Phe506) provide a preference for strong ribonucleotide discrimination.[86,128] The corresponding motif in Pol μ is replaced with a Gly435–Trp436.[129] Prior to the completion of the crystal structure of Pol μ, sequence alignment analysis coupled with site-directed mutagenesis identified the amino acid residue Gly435 of Pol μ as the residue is critically responsible for this enzyme's lack of sugar discrimination during incorporation into single-nucleotide gapped DNA. This is probably because the small side chain of Gly435 does not act as a steric barrier for the 2′-OH of an incoming rNTP.[130] Single amino acid substitutions have also been used to examine the basis of sugar selectivity for a number of other polymerases.[131–135]

Countless studies on Pol β mutants lend insight into the role of individual side chains in binding and catalysis (reviewed in Beard and Wilson[83]). Specifically, mutagenesis has been used to examine the active-site interactions of Asp276 with incoming dNTP, Lys280 with the templating base, and Tyr271, Asn279, and Arg283 with the minor groove edge of DNA in proximity to the nascent base pair binding pocket. Individual mutagenesis of Pol β catalytic residues Asp190, Asp192, and Asp256 abolishes polymerase activity, and gave first clues as to their active-site location and critical role in catalysis prior to structural information availability.[136,137] Two site-specific Pol β mutants, R258A and I260Q (discussed below), have been used to further dissect the mechanism of Pol β nucleotide incorporation.[138,139]

8.10.4.1.4 Continuous transient-state kinetic methods (stopped-flow assays)

Perhaps the largest advances in elucidating the kinetic mechanism of DNA polymerases have been obtained using stopped-flow technique and various fluorescent probes. For example, use of a fluorophore-modified DNA substrate has facilitated real-time visualization of conformational changes that occur during the course of dNTP incorporation catalyzed by a number of DNA polymerases, including Pol β, KF, Dbh, and T4 DNA polymerase.[138,140–144] Alternatively, a fluorophore can be attached to the polymerase itself and serve as an independent reporter of changes in enzyme conformation.[145] The significant advantage of the stopped-flow fluorescence method is that it allows direct measurement of the rate of intermediate species formation and disappearance. Application of various substrate analogues and alteration of the reaction conditions in fluorescence stopped-flow studies of Pol β result in a most complete understanding of DNA polymerase kinetic mechanism (as described in Section 8.10.4.2).

Development of fluorescence resonance energy transfer (FRET) systems have provided perhaps the most direct way of determining the rate of the 'open-to-closed' conformational change in DNA polymerase mechanism.[146–148] A single fluorescent probe (such as fluorophore-modified DNA or a fluorophore-labeled enzyme) might reflect both global and local structural changes, which makes interpretation of results from stopped-flow fluorescence methods more complex and, in some cases, ambiguous. In contrast, a pair of strategically positioned donor/acceptor fluorescence probes can serve as immediate reporters of DNA polymerase global conformational changes, as changes in distance between the two fluorophores upon the motion of the enzyme subdomains result in changes of FRET efficiency.

8.10.4.1.5 Single molecule kinetics

T7 DNA polymerase was the first polymerase studied at the single molecule level.[149] In these studies DNA substrate was labeled with a Cy3 fluorescent probe that is known to be sensitive to changes in the environment. Addition of correct dNTP triggers a change in E•D$_n$ binary complex conformation, which results in an increase in Cy3 fluorescence. Notably, no increase of fluorescence intensity was observed on the single-molecule level in the absence of dNTP substrate. This observation argues against the hypothesis that the binary E•D$_n$ complex exists in a dynamic equilibrium between 'open' and 'closed' conformational states and that dNTP binding shifts the equilibrium toward the 'closed' state.[150] Therefore, it is probable that dNTP binding is absolutely required for the initiation of the conformational change. Importantly, the results of the single molecule kinetics correlate perfectly with the results of stopped-flow ensemble-averaged assays using the same Cy3 modified DNA substrate.[149]

8.10.4.2 DNA Polymerase Kinetic Mechanism

Pol β is possibly the best-studied DNA polymerase to date, and we present it here as a model enzyme to illustrate current progress in the field. Our current knowledge of the DNA polymerase kinetic mechanism can be illustrated by **Figure 4** and is summarized as follows. Binding of dNTP to E•D$_n$ binary complex (step 1) induces fast N-subdomain closing (step 2). This step remains mostly unperturbed for both matched and mismatched nucleotide incorporation. Active-site residue rearrangements during the course of the subdomain-closing conformational change create a binding pocket for the catalytic Mg^{2+} ion (step 3). There is no evidence for a kinetically distinct rate-limiting conformational step induced by catalytic Mg^{2+} binding. Instead, the chemistry step (step 4) for both matched and mismatched incorporation is rate limiting through phosphodiester bond formation. However, the mismatched E′•D•N•M complex is substantially destabilized in

comparison to the matched E′•D•N•M complex. The free energy difference between these complexes is further enhanced through the chemical transition state. Catalytic Mg^{2+} dissociation (step 5), subdomain reopening (step 6), and pyrophosphate dissociation (step 7) follow phosphodiester bond formation to complete a single turnover of dNTP incorporation. In the following subsections, experimental evidence for this proposed scheme is presented. It must be clarified that for purposes of discussion in this chapter, inclusive to the chemical step are all microscopic steps pertaining to both enzyme and substrate active-site adjustments through nucleotidyl transfer, from E′•D_n•N•M to E′•D_{n+1}•P•M in **Figure 4**. Computational studies (Section 8.10.5) have been used to further investigate these kinetically unresolvable microscopic steps within the chemistry step.

8.10.4.2.1 Stopped-flow fluorescence

Stopped-flow fluorescence analyses of Pol β have been very important in advancing DNA polymerase mechanism.[89,138,140,144,151] Commonly used in DNA polymerase studies is 2-aminopurine (2-AP) – a fluorescent probe, which acts as an excellent analogue of adenine in forming an almost undistorted pair with thymidine (**Figure 9**). It has been suggested that changes in aromatic stacking within DNA dominate the fluorescence emission of 2-AP.[152] Crystal structures of Pol β binary and ternary complexes reveal that the templating position downstream from the nascent base pair experiences dramatic changes in base-stacking interactions during the course of a single turnover.[78] Consequently, a DNA substrate with 2-AP occupying this position (**Figure 9**) yields the greatest signal-to-noise ratio for 2-AP emission in DNA polymerase fluorescence studies.[140] This is probably due to the 90° DNA backbone kink observed in the closed ternary structure which minimizes the base-stacking interactions of 2-AP in this position with the preceding and following bases.

For purposes of the discussion in the following sections, unless otherwise specified, a typical stopped-flow reaction is initiated by rapid mixing of preformed E•D_n binary complex with Mg•dNTP in the presence of excess Mg^{2+}. Monitoring of 2-AP fluorescence (present in the DNA substrate) during correct dNTP incorporation in stopped-flow results in a biphasic trace, in which one phase has a rate identical to that of single dNTP incorporation (as determined by rapid chemical quench experiments) and the other phase has a significantly faster rate (**Figure 10**). Importantly, use of fluorescence from tryptophan, naturally present in the N-subdomain of Pol β, as an independent probe of Pol β conformational changes, also reveals a biphasic fluorescence transition possessing rates similar to those obtained in 2-AP fluorescence stopped-flow assays.[140,151] This observation indicates that both fluorophores report the same steps in Pol β reaction pathway.

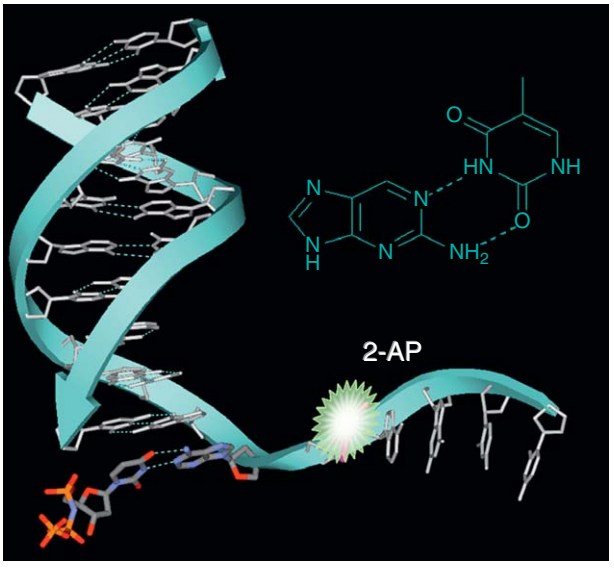

Figure 9 Position of 2-AP fluorescent probe in DNA substrate from Pol β ternary complex structure 2FMS as reported in V. K. Batra; W. A. Beard; D. D. Shock; J. M. Krahn; L. C. Pedersen; S. H. Wilson, *Structure* **2006**, *14*, 757–766. Right corner: Structure of 2-aminopurine base-paired with thymidine.

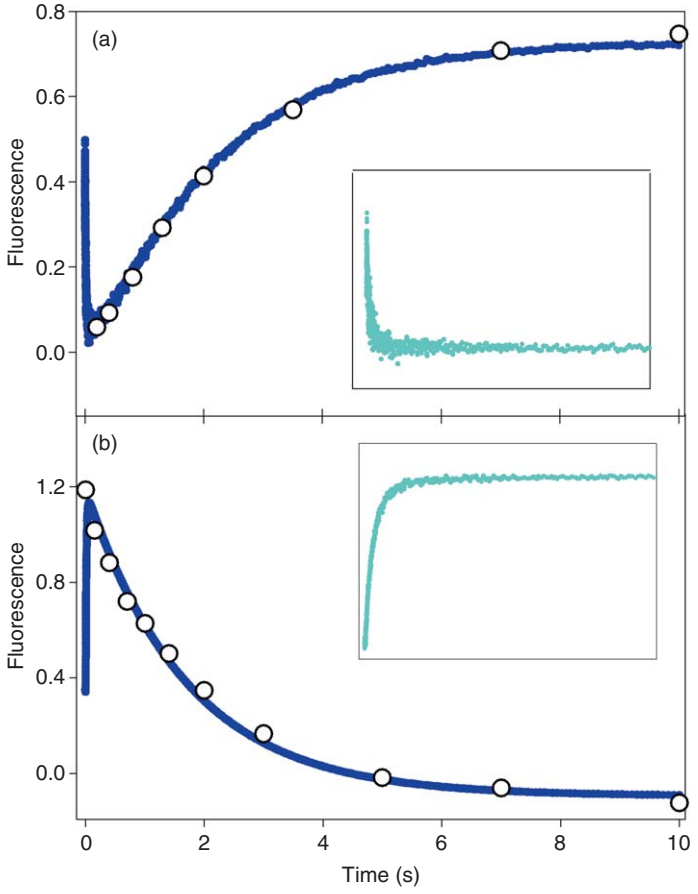

Figure 10 Superimposition of rapid chemical quench (open circles ○) and stopped-flow fluorescence (blue) assays. In (a) tryptophan emission was detected, and in (b) the fluorescence change from 2-AP was monitored. Insets show the dNTP binding-induced conformational change in the presence of dideoxy-terminated DNA substrate. Adapted with permission from A. K. Showalter; B. J. Lamarche; M. Bakhtina; M. I. Su; K. H. Tang; M. D. Tsai, *Chem. Rev.* **2006**, *106*, 340–360. Copyright 2006 American Chemical Society.

8.10.4.2.2 Structural bases of the fast and slow fluorescence transitions

In order to delineate the structural bases of the fast and slow fluorescence transitions, further studies involving a variety of chemical probes and altered reaction conditions have been conducted:

1. Traces from stopped-flow experiments utilizing natural dNTP in combination with dideoxy-terminated DNA substrate, in which the 3′-OH of the primer terminus is absent, do not exhibit the slow phase of fluorescence transition (**Figure 10**, inset). Since nucleotidyl transfer is not possible with dideoxy-terminated DNA substrate, the existence of fast fluorescence transition alone indicates that the fast phase of the stopped-flow trace is associated with a conformational step preceding chemistry, while completion of the chemical step is required for the slow phase to appear.[89,140,151] Similarly, the presence of only the fast phase is observed in stopped-flow experiments utilizing the combination of regular nondideoxy-terminated DNA substrate and nonhydrolyzable α,β-methylene-dNTP (dNMPCPP) analogues.[153]
2. It is generally accepted that thio-substituted analogues (S_p-dNTPαS) should perturb mainly the chemical step rather than conformational steps. Use of thio-substituted analogues in stopped-flow assays show that the rate of the fast phase remains unperturbed, while the rate of the slow fluorescence transition is significantly reduced (**Figure 11(a)**).[151] This reinforces the association of the rate of the slow fluorescence transition with the rate of chemistry.

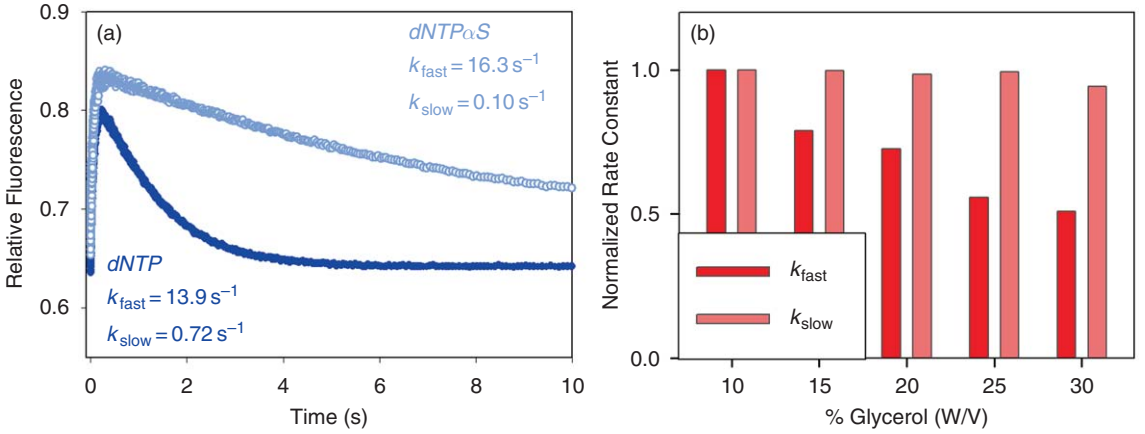

Figure 11 (a) Effect of dNTPαS in 2-AP stopped-flow fluorescence assays. Reproduced with permission from M. Bakhtina; S. Lee; Y. Wang; C. Dunlap; B. Lamarche; M. D. Tsai, *Biochemistry* **2005**, *44*, 5177–5187. Copyright 2005 American Chemical Society. (b) Viscosity effect on the fast and slow fluorescence transitions. Adapted with permission from M. Bakhtina; M. P. Roettger; S. Kumar; M. D. Tsai, *Biochemistry* **2007**, *46*, 5463–5472. Copyright 2007 American Chemical Society.

3. Viscogens, such as glycerol, can be used to perturb conformational steps in an enzymatic pathway which involve large spatial motions.[154–157] Viscosity studies at neutral pH indicate that upon increasing sucrose or glycerol concentrations in the reaction buffer, the fast fluorescence transition significantly slows down, while the rate of the slow fluorescence transition remains virtually unaffected (**Figure 11(b)**).[151] This selective sensitivity to the presence of a viscogen suggests that the fast fluorescence transition reflects a major conformational change associated with progression from the 'open' binary to the 'closed' ternary complex (step 2 in **Figure 4**). Also, the rate of the slow phase does not show sensitivity to altered buffer viscosity, as would be expected of a step reflecting the rate of chemistry.
4. On the basis of negligible structural changes observed between the Pol β pre-chemistry ternary complex and the Pol β post-chemistry ternary complex prior to pyrophosphate release,[89] it is important to point out that the slow fluorescence transition is not caused by the phosphodiester bond formation directly. Instead, the fluorescence change originates from a conformational change rate limited by chemistry. In other words, this conformational step should occur after chemistry with a rate faster than chemistry.

   Examination of the effects of pH on Pol β dNTP incorporation demonstrate that as pH increased, the rate of the fast fluorescence phase remains mostly unchanged, while the rate of the slow fluorescence phase increases considerably.[138] Hence, under conditions of high pH (green profile in **Figure 12**), the energy barrier of the chemical step is lowered relative to that at neutral pH (blue profile in **Figure 12**),

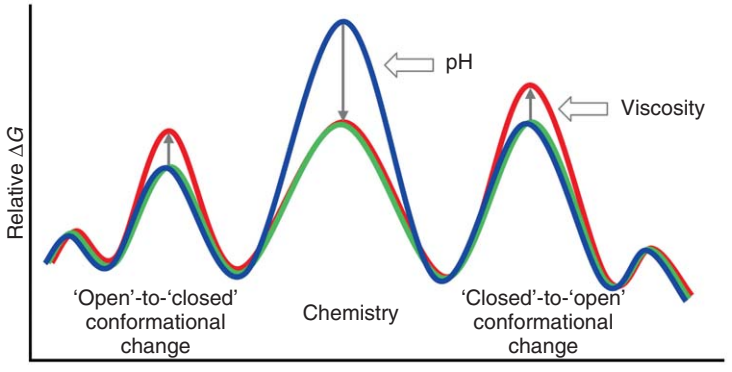

Figure 12 Qualitative free energy profile of correct dNTP incorporation by Pol β. This figure depicts Pol β mechanism at neutral pH (blue), high pH (green), and high pH and high viscosity (red). Adapted with permission from M. Bakhtina; M. P. Roettger; S. Kumar; M. D. Tsai, *Biochemistry* **2007**, *46*, 5463–5472. Copyright 2007 American Chemical Society.

becoming comparable to the energy barriers of the conformational steps. As discussed above, viscosity can selectively affect the rate of conformational steps, so that as reaction buffer viscosity increases, the rate of the fast fluorescence transition decreases. Therefore, selective slowing of the conformational steps (through increased buffer viscosity) in combination with a selective increase in chemistry (through increased pH) should yield conditions in which a conformational change, rather than chemistry, has the highest energy transition step (red profile in **Figure 12**) during the course of single-nucleotide incorporation.

In agreement with this proposal, results of stopped-flow assays performed at high pH demonstrate that both fast and slow fluorescence transitions are sensitive to increased buffer viscosity, which indicates that chemistry does not limit the rate of the slow phase under these conditions (**Figure 13(a)**). Notably, the rate of dNTP incorporation determined in rapid chemical quench remains unaffected by increases in viscosity (**Figure 13(b)**). Hence, under conditions of high pH and high viscosity, the rate of single dNTP incorporation is faster than the rate of the second fluorescence change. The concomitant effects of pH and viscosity used to dissect the rate of chemistry and the rate of the slow fluorescence change observed in stopped-flow during dNTP incorporation lend support to the hypothesis that the slow fluorescence transition actually originates from N-subdomain reopening after chemistry (step 6 in **Figure 4**).[138] Similar conclusions have been obtained from kinetic analyses of KF and Dpo4 DNA polymerases;[138,158] however, for these enzymes the rate of the reopening from the closed conformation is slower than the chemical step under neutral pH conditions.

5. Site-directed mutagenesis has been successfully utilized to further support the assignment of the slow fluorescence transition to the N-subdomain reopening step.[138] Comparison of crystal structures of Pol β binary, ternary, and product complexes demonstrates that dNTP-induced conformational closing and reopening after dNTP incorporation are accompanied by Arg258 side-chain reorientation.[78] Recent computational studies have suggested that Arg258 side-chain reorientation is probably the rate-limiting microscopic event during the course of Pol β's subdomain closing before chemistry and reopening after chemistry.[159,160] It has also been proposed that the R258A mutant has a lower energy barrier for the subdomain-closing and reopening steps compared to wild type (WT). Stopped-flow fluorescence analyses of R258A indicate that the mutant enzyme has a facilitated rate for the conformational step responsible for the origin of the slow fluorescence transition, which further supports that the slow fluorescence transition results from Pol β's N-subdomain-reopening step.[138]

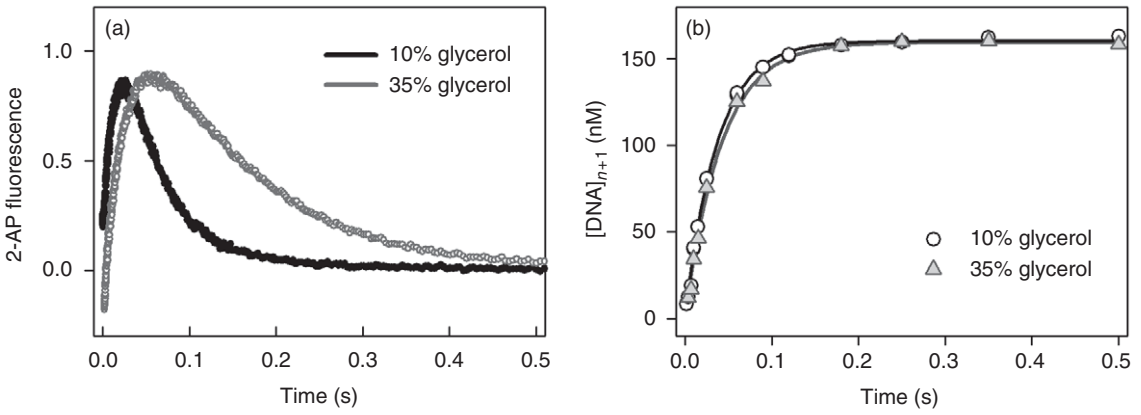

Figure 13 Comparison of Pol β catalyzed single-nucleotide incorporation at 10% and 35% glycerol, pH 8.3. (a) 2-AP fluorescence stopped-flow assays show that both phases of the fluorescence change are slowed down at increased glycerol concentration. (b) In contrast, rapid chemical quench assays demonstrate that the rate of nucleotide incorporation remains unaffected by the altered glycerol concentration. Adapted with permission from M. Bakhtina; M. P. Roettger; S. Kumar; M. D. Tsai, *Biochemistry* **2007**, *46*, 5463–5472. Copyright 2007 American Chemical Society.

8.10.4.2.3 Kinetic analysis of 2-AP fluorescence stopped-flow data

Having the two fluorescence transitions assigned to certain steps in a kinetic scheme, it is possible to extract kinetic constants from the dependence of the stopped-flow traces on dNTP concentration. Typically, the amplitude of fluorescence change and rates of fast and slow phases increase as the concentration of dNTP increases (**Figure 14**). The closed E′•D_n•N and E′•D_{n+1}•P complexes have a higher intensity of 2-AP fluorescence emission compared to binary E•D_n and E•D_{n+1} complexes (as well as open E•D_n•N and E•D_{n+1}•P); therefore, upon increasing dNTP substrate concentration the increasing observed fluorescence amplitude signifies an increasing concentration of closed ternary complex, a pattern entirely consistent with the general polymerase kinetic mechanism depicted in **Figure 4**.

In agreement with the kinetic scheme, rates for both fast and slow fluorescence transitions show a hyperbolic dependence on dNTP concentration. For fast-phase analysis, observed rate constants plotted as a function of dNTP concentration should fit to a hyperbolic equation with a nonzero intercept.[139,144] According to the Pol β kinetic mechanism (**Figure 4**), fitting reveals values for the microscopic rate constant k_2 (conformational closing step) and dNTP thermodynamic dissociation constant $K_d = k_{-1}/k_1$. For slow-phase analysis, dNTP concentration dependence should fit to a simple rectangular hyperbola, and kinetic parameters obtained from this analysis correspond to k_{pol} and $K_{d,app}$ from single-turnover rapid chemical quench assays. Note again, that interpretation of the parameters obtained from kinetic analyses depends on the particular proposed kinetic scheme and could be inappropriate for certain DNA polymerases. One such case is Pol X (mentioned in Section 8.10.4.1.1), which binds dNTP prior to DNA substrate. The fast 2-AP fluorescence transition in Pol X stopped-flow studies corresponds to conformational rearrangements upon DNA binding to Pol X•dNTP binary complex.[113]

8.10.4.2.4 Measurement of the reverse rate of the conformational step

Conformational closing of the N-subdomain requires binding of the nucleotide substrate in complex with a divalent metal ion. Sequestering of Mg^{2+} by addition of EDTA eliminates the Mg•dNTP substrate from the reaction and thus shifts the equilibrium of the conformational step toward the open conformation (step 2 in **Figure 4**), which allows direct measuring of the reverse rate k_{-2}.[153] When the stopped-flow reaction is initiated by rapid mixing of preformed E′•D_n•N ternary complex with excess EDTA, the observed 2-AP fluorescence change (**Figure 15**, pink trace) has the direction opposite to that elicited by the forward conformational closing initiated by mixing preformed E•D_n binary complex and Mg•dNTP (**Figure 15**, dark blue trace). Importantly, in the case of Pol β, the rate of reverse opening (k_{-2}) is faster than or comparable to the rate of the chemical step

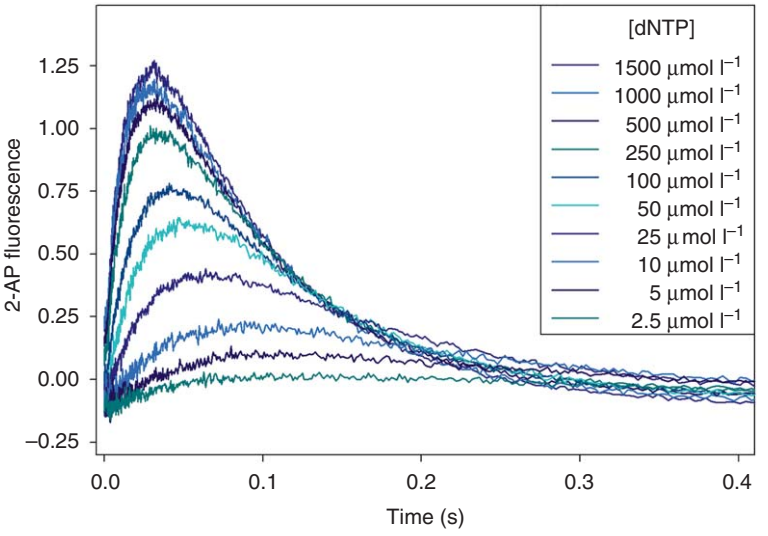

Figure 14 Concentration dependence of correct dNTP incorporation as monitored by stopped-flow 2-AP fluorescence assays.

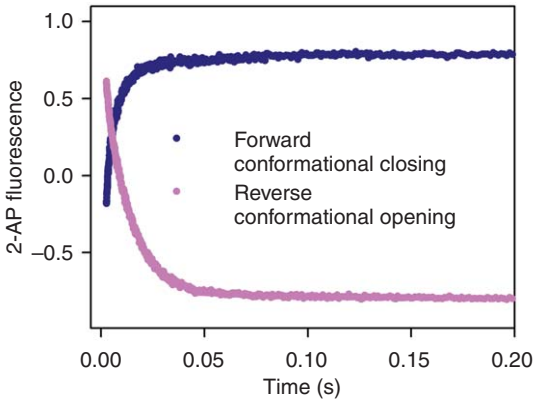

Figure 15 Forward conformational closing (dark blue) and reverse conformational opening (pink) as monitored by stopped-flow 2-AP fluorescence assays. Adapted with permission from M. Bakhtina; M. P. Roettger; M. D. Tsai, *Biochemistry* **2009**, *Submitted.* Copyright 2009 American Chemical Society.

(k_3). This result reinforces that the highest energy transition state of Pol β's reaction pathway corresponds to the chemical transition state and highlights the key role of chemistry in the fidelity of Pol β. Interestingly, the reverse opening rate of T7 DNA polymerase is quite slow relative to chemistry, suggesting that the conformational step plays a determining role in fidelity of this polymerase.[145,161]

8.10.4.2.5 Pol β kinetic mechanism summary and comparison with other DNA polymerases

The results of the aforementioned stopped-flow fluorescence studies of Pol β support the proposed model in **Figure 4**. It is worth noting that the relative energy barriers for chemical and conformational steps might be influenced by a number of factors such as pH, viscosity, DNA sequence, and interactions with other proteins. For instance, the stopped-flow results for Pol β suggest that the subdomain-closing step is faster than the rate of single-nucleotide incorporation by a factor of 100 at pH 6.1 and by less than a factor of 3 at pH 8.5. Obviously, the relative rates could differ for different DNA polymerases. However, there is evidence for a fast conformational change during correct dNTP incorporation among other DNA polymerases. Direct monitoring of N-subdomain motions in Klentaq1, using FRET, indicate that the subdomain closing is substantially faster than the rate of single-nucleotide incorporation.[147] Stopped-flow fluorescence and FRET studies of KF revealed fast dNTP binding-induced conformational changes prior to phosphodiester bond formation.[138,142,146] Besides the above empirical studies, recent computational analysis of the free energy landscape for correct and mismatched nucleotide incorporation by T7 DNA polymerase also indicate that the chemical step is rate limiting.[162] Nevertheless, even though current experimental and computational data are consistent with the model that chemistry is the rate-limiting step through phosphodiester bond formation for several DNA polymerases, it would be too hasty to conclude a common rate-limiting step for all members of this class of enzymes.

8.10.4.3 Dissection of the Role of Two Metal Ions

8.10.4.3.1 Use of exchange-inert metals in stopped-flow analysis

In addition to characterization of the two phases observed in stopped-flow fluorescence assays during Pol β correct nucleotide incorporation, studies using exchange-inert chromium(III) and rhodium(III) dNTP complexes have been able to further examine the order of magnesium ion binding in the active site during catalysis. Unlike Mg^{2+} nucleotide complexes, which are in rapid equilibrium in aqueous solution (with exchange rates of $5000\,s^{-1}$),[163] exchange-inert nucleotide complexes have ligand exchange rates measured in days under non-basic conditions.[164] Enzyme binding of two magnesium ions, namely consisting of a nucleotide-binding Mg^{2+} and a catalytic Mg^{2+} (as described in Section 8.10.3.3 and **Figure 3**), is a requirement for catalysis. Binding of

exchange-inert Cr(III)•dNTP to Pol β•DNA binary complex in the absence of Mg^{2+} induces the fast phase of fluorescence alone. Upon subsequent addition of Mg^{2+} the slow phase of fluorescence is restored.[165] Similarly, mixing of preformed Pol β•DNA•Rh(III)dNTP ternary complex with Mg^{2+} results in the slow fluorescence phase only. Upon mixing of Mg^{2+} with preformed Pol β•DNA•Rh(III)dNTP ternary complex in which the DNA primer is dideoxy-terminated, no stopped-flow signal is observed at all.[151] All of these results suggest that a fast conformational change (step 3, **Figure 4**) occurs upon metal•dNTP binding to the E•D_n binary complex, and support that binding of the catalytic Mg^{2+} (step 4, **Figure 4**) occurs after the formation of the E′•D_n•N ternary complex.

To address the possibility of obtaining unnatural results through use of the exchange-inert metal•dNTP complexes mentioned above, the respective difference in binding affinity for each of the two magnesium ions ($K_{d,app}{}^{Mg^{2+}} = 1.0\,mmol\,l^{-1}$ and $K_{d,app}{}^{Mg\bullet dNTP} = 46\,\mu mol\,l^{-1}$)[140] was employed to further test the Mg^{2+} binding order.[151] Stopped-flow results showed that upon rapid mixing of Pol β•DNA with dNTP under limiting magnesium concentrations which allow Mg•dNTP binding site saturation, yet do not provide sufficient Mg^{2+} to support catalysis, only the fast phase of fluorescence transition was observed. Paralleling the rhodium(III) experiments mentioned above, fluorescence monitoring of Pol β•DNA•MgdNTP ternary complex, preformed under limited magnesium concentration so as to prevent chemistry and then mixed with excess Mg^{2+}, demonstrates only the slow fluorescence transition as well. Such results with the use of Mg^{2+} instead of its analogues further corroborate conclusions of the mechanism studies using exchange-inert metal•dNTP complexes.

8.10.4.3.2 Structural evidence for order of metal binding

Further validation regarding the metal binding order proposed for the Pol β mechanism is found in the crystal structure of pathway intermediate, Pol β•DNA•Cr(III)dTMPPCP.[89] This ternary structure represents a fully functional pre-chemistry intermediate, as the primer retains the 3′OH and the product complex was observed upon soaking of the crystals in a solution containing divalent metal ion. Notably, in the absence of a bound catalytic metal ion, Pol β is found in a fully closed conformation. Importantly, this finding provides structural support to the conclusions from the aforementioned stopped-flow studies confirming that M•dNTP binding is sufficient to induce N-subdomain closure with no requirement for catalytic Mg^{2+} binding.

8.10.4.4 Mismatched dNTP Incorporation

Polymerase fidelity, defined by the ratio of the catalytic efficiencies for correct and incorrect dNTP incorporations, is governed by the free energy difference between the highest energy barriers along the correct and incorrect dNTP incorporation pathways. Since fidelity requires knowledge of both pathways, the disproportion of structural and mechanistic information available for matched dNTP incorporation compared with that for mismatched dNTP incorporation, gives rise to an ambiguous understanding of the molecular mechanism of DNA polymerase fidelity.[166,167] It must be noted that the means by which mismatch discrimination is accomplished is probably both polymerase and mispair specific. A variety of deviant kinetic pathways have been suggested for misincorporation among polymerases,[142,145,162,168–170] in which either: (1) mismatched dNTP incorporation occurs through a distinctly different pathway than matched dNTP, or (2) mismatched dNTP and matched dNTP incorporations proceed through analogous kinetic pathways, in which the energetics of the transition states and intermediate complexes differ. In either case, the presence of a mismatch within the active site probably generates a perturbed ternary complex conformation.

Gaining structural insights into the mismatched dNTP mechanism is a difficult task since true mismatched ternary complexes (E′•D_n•N•M, **Figure 4**) are not readily crystallized due to inherent thermodynamic instability. However, first insights into mismatch incorporation for various polymerases were resolved through complexes depicting mispairs within the active site[169,171] and mismatch extension.[172,173] For example, a post-chemistry structure of Pol β complexed with a nicked DNA substrate containing a terminal mispair shows only partial closing of the α-helix N, and a staggered arrangement of the terminal bases rather than normal Watson–Crick base pairing.[169] On the basis of these structures, it was proposed that mismatched dNTP incorporation may occur with a partially open N-subdomain conformation. Recently, a high-resolution functional pre-chemistry closed ternary complex for Pol β with an incoming mismatched nonhydrolyzable dAMPCPP demonstrates that the enzyme remains in a fully closed conformation comparable to that observed for matched

dNTP.[174] In the active site of this structure, however, the template DNA is shifted in order to accommodate the mismatched dNTP, such that no coding template base is in the nascent base pair binding pocket. The aberrant positioning of the DNA provides structural evidence for the mechanism of Pol β's inefficient misincorporation, as the 3′-OH of the primer, Pα of the incoming dNTP, and catalytic metal ion, do not demonstrate proper active-site geometry. It has been suggested that minor adjustments of active-site residues are required to bring about proper active-site geometry for catalysis, and that these local adjustments may play a critical role in defining Pol β's fidelity.[175,176]

In general, as discussed above, in the presence of a mismatch the polymerase active site does not fit properly as in Watson–Crick pairing, and catalysis is unfavorable due to less than ideal active-site geometry. As a result of improper alignment, polymerases generally incorporate mismatches with slower rates (smaller k_{pol}) and bind mismatched dNTP loosely (larger $K_{d,app}$ values).[107] Kinetic data for mismatched dNTP incorporations by many DNA polymerases have been reported using rapid chemical quench,[11,102,106,177–180] yet this commonly used kinetic approach does not allow characterization of individual steps in the mismatched dNTP incorporation pathway. To circumvent this, transient kinetic methods (as have been discussed in Sections 8.10.4.1 and 8.10.4.2 for matched dNTP incorporation), including stopped-flow and FRET, have been applied to examine mismatch incorporation, and they reveal important information about conformational motions of polymerases occurring during mismatch catalysis as highlighted in the following sections.

8.10.4.4.1 Mismatched and matched dNTP incorporation occur through analogous kinetic pathways

1. *Stopped-flow fluorescence reveals a fast conformational change for mismatched dNTP incorporation.* Recently, as an extension of previous methodology used to delineate Pol β's correct dNTP incorporation mechanism,[138,140,151] stopped-flow fluorescence and steady-state fluorescence spectroscopy have been employed to examine the mechanism of mismatched dNTP incorporation by Pol β.[139] These studies led to the conclusion that there is probably a conformational closing event that occurs for mismatched dNTP incorporation, as evidenced by the existence of a fast fluorescence phase preceding chemistry. In addition, the rate of the conformational change induced by mismatched dNTP was comparable to that of N-subdomain closing induced by correct dNTP. Furthermore, steady-state fluorescence studies demonstrated that both matched and mismatched dNTP elicit the same direction of fluorescence change (**Figure 16(a)**).

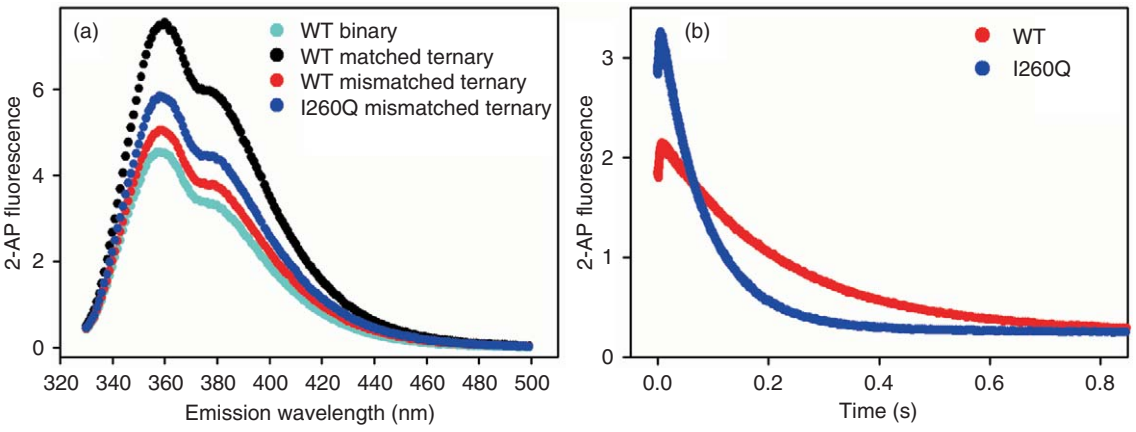

Figure 16 (a) Steady-state fluorescence spectra of matched and mismatched ternary complexes for WT Pol β and I260Q. Emission spectra shown include WT binary complex (cyan), WT T:A matched ternary complex (black), WT T:G mismatched ternary complex (red), I260Q T:G mismatched ternary complex (blue). Omitted for simplification are the I260Q binary and T:A matched ternary complexes, which overlay accurately with the corresponding WT traces. (b) Comparison of WT Pol β and I260Q T:G mismatched incorporation as monitored by 2-AP fluorescence assays. Reproduced with permission from M. P. Roettger; M. Bakhtina; M. D. Tsai, *Biochemistry* **2008**, *47*, 9718–9727. Copyright 2008 American Chemical Society.

Previous stopped-flow fluorescence assays investigating matched dNTP incorporation showed that both the fast and the slow fluorescence transitions demonstrated a hyperbolic dependence on dNTP concentration.[140,144] Similarly, the dNTP dependence of both the fast and the slow fluorescence phases during mismatched dNTP incorporation in stopped-flow has been examined. The observed rate constants for the fast and the slow phases, individually plotted as a function of dNTP concentration, reveal that both phases demonstrate a hyperbolic dependence on dNTP concentration (parameters obtained for k_2, K_d, k_{pol}, and $K_{d,app}$ as described in Section 8.10.4.2.3 and reported in **Table 1**). The observed hyperbolic dependence of the fast phase on mismatched dNTP largely indicates that this phase originates from a conformational change induced by mismatched dNTP binding.

Overall, all the aforementioned results support that, analogous to the prior assignments for correct dNTP incorporation, the fast and slow fluorescence changes observed for mismatched incorporation (**Figure 16(b)**) can be assigned to the dNTP-induced subdomain-closing conformational change and the chemical step (which probably limits the reopening step), respectively. An important observation is that the forward rate of conformational closing (k_2, **Figure 4**) for mismatched dNTP incorporation is comparable with that for correct dNTP incorporation (though with significant increase in K_d), while the maximum rate of nucleotide incorporation (k_{pol}) is substantially slower (also with significant increase in $K_{d,app}$) (**Table 1**). This suggests that overall mismatched incorporation follows a similar pathway, though both the K_d and $K_{d,app}$ values are higher and the rate of the chemical step is slower. These results are further supported by the ternary mismatch structure of Pol β which exists in the closed form.[174]

The observation that the conformational change occurs with a similar rate for both correct and mismatched incorporation by Pol β differs from the conclusion of the recent single molecule kinetic analysis of T7 DNA polymerase,[149] which reported a significantly reduced rate of conformational closing induced by mismatched dNTP binding. However, another study on T7 reported little difference in the forward rates of conformational closing between matches and mismatches, while noting a large difference in the reverse rates of conformational closing.[145] Additional studies on KF,[142] Dbh,[141] and T4[181] utilizing 2-AP fluorescence conclude on the basis of differences in fluorescence signals between matched and mismatched dNTP, so that there may exist distinctly different misincorporation pathways. It remains to be established whether such discrepancy reflects differences in the mismatched discrimination mechanism employed by various polymerases, or whether it results from different experimental systems and conditions.

Table 1 Kinetic comparison of rate and binding constants for WT versus I260Q for matched and mismatched dNTP incorporation

	dT:dA (matched)		*dT:dG (mismatched)*	
	Wild Type	*I260Q*	*Wild Type*	*I260Q*
K_2 (s^{-1})	116 ± 5	108 ± 7	256 ± 8	485 ± 25
K_d ($\mu mol\,l^{-1}$)	29.5 ± 3.6	6.57 ± 2.12	488 ± 103	232 ± 37
k_{pol} (s^{-1})	42.9 ± 0.6	43.6 ± 1.4	5.70 ± 0.11	13.6 ± 0.2
$K_{d,app}$ ($\mu mol\,l^{-1}$)	6.79 ± 0.48	7.07 ± 1.20	489 ± 26	48.8 ± 2.5
$k_{pol}/K_{d,app}$[a]	6.32	6.17	0.0117	0.279
Fidelity[b]	–	–	541	23.1

[a] Catalytic efficiency measured in units $s^{-1}\,\mu mol^{-1}\,l$.

[b] Fidelity defined as $[(k_{pol}/K_{d,app})_{cor} + (k_{pol}/K_{d,app})_{inc}]/(k_{pol}/K_{d,app})_{inc}$ – where the subscripts 'cor' and 'inc' indicate the correct (matched) and incorrect (mismatched) nucleotide incorporation, respectively.

The k_2, K_d, k_{pol}, and $K_{d,app}$ values were obtained from hyperbolic fit of the dNTP concentration dependence of the observed rates of the fast and slow fluorescence phases as described in Section 8.10.4.2.3. The k_2 value represents the rate constant of forward conformational closing, while K_d reflects the stability of the ternary complex before closing. Therefore, WT and I260Q show little difference during initial dNTP binding before the conformational change. The k_{pol} value represents the maximum rate of dNTP incorporation, while the $K_{d,app}$ value possesses a contribution from all steps up to the rate-limiting step and can be thought as the dissociation constant of the closed ternary complex.

2. *Rate-limiting chemistry for matched and mismatched dNTP incorporation.* Comparative kinetic analyses of Pol β strongly support that the chemistry step is rate limiting for both matched and mismatched incorporation pathways.[139] Similarly, results of linear free energy relationship (LFER) studies utilizing dNTP analogues, in which the β,γ-bridging oxygen is substituted with various halomethylene moieties, suggests that for both matched and mismatched incorporation P–O bond breaking makes a significant contribution to the rate-limiting step.[118,119] Based on the observation that the Brønsted correlation between log k_{pol} and the leaving group pK_a for monohalogenated analogues is very similar between correct and incorrect dNTP incorporations, it is concluded that the corresponding transition states have similar positions on the free energy surface. However, notably different Brønsted correlations observed with bulkier dihalogenated analogues suggest the existence of structural differences at the chemical transition states of correct and mismatched incorporations. In addition, analysis of pH dependence and solvent deuterium isotope effects revealed that a proton transfer step (steps) might be at least partially rate limiting for both matched and mismatched dNTP insertion.[119] Overall, these results support the proposal that the rate-limiting chemical step is a major contributor to Pol β fidelity.[167]

8.10.4.4.2 Correlation between fidelity and mismatched transition state destabilization

Site-directed mutagenesis allows us to investigate fidelity variances consequent of single residue mutations of a single polymerase. The Ile260 residue of Pol β is located in the hydrophobic hinge region between the C- and the N-subdomains.[77,87] The mutator activity of site-directed mutant I260Q was first identified by a genetic screen,[182] and subsequent pre-steady-state kinetic characterization showed that it possessed a low fidelity due to loose binding discrimination of mismatched dNTP substrates.[183] These characteristics make the I260Q mutant of specific interest in fidelity studies of Pol β, in order to further understand how one mutation can alter the mismatch discrimination profile of this enzyme. Mechanistic studies using stopped-flow fluorescence demonstrated both enzymes possess similar correct dNTP incorporation profiles (**Figure 17**, black profile), and that the main difference between I260Q and WT lies in the ability of I260Q to more efficiently stabilize the mismatched ternary complex, as suggested by the 10-fold decrease in $K_{d,app}$ of I260Q ($48.8 \pm 2.5\ \mu mol\ l^{-1}$) relative to WT ($489 \pm 26\ \mu mol\ l^{-1}$) for dT:dG mismatch incorporation (**Table 1**). This was further corroborated by an observed higher amplitude for I260Q in stopped-flow fluorescence traces and steady-state emission spectra for mismatched dNTP (**Figure 16**).[139] Overall, comparison studies between WT Pol β and the lower fidelity I260Q variant illustrate the correlation between fidelity and mismatch destabilization, as the infidelity of I260Q originates from enhanced stabilization of the mismatched ternary complex and the chemical transition state (**Figure 17**, blue trace).[139] These results strongly support that both matches and mismatches are incorporated through analogous mechanisms, and that the fidelity of Pol β is controlled, at least partly, by

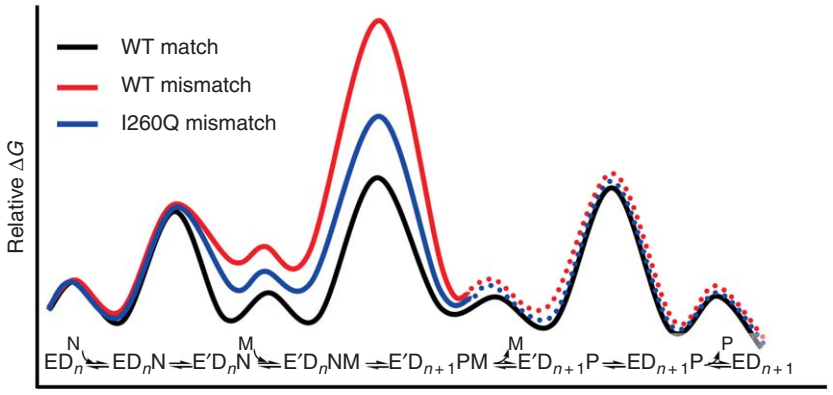

Figure 17 Qualitative free energy profile of matched and mismatched dNTP incorporation by WT Pol β versus I260Q. E = DNA polymerase in open conformation; E′ = closed conformation; D_n = DNA; N = Mg•dNTP; M = catalytic Mg^{2+}; P = Mg•PP_i. Reproduced with permission from M. P. Roettger; M. Bakhtina; M. D. Tsai, *Biochemistry* **2008**, *47*, 9718–9727. Copyright 2008 American Chemical Society.

destabilization of the mismatched ternary complex and the chemical transition state in the same reaction pathway (Figure 17, red profile).

The observation of an incorrect dNTP-induced conformational change by Pol β may appear to contradict the findings of two FRET-based studies monitoring the conformational motions of Klentaq[147] and KF.[148] Both studies report an increase in FRET signal, upon addition of correct dNTP, yet do not observe any noticeable change upon addition of incorrect dNTP. In contrast to moderate and low-fidelity polymerases, including Pol β, since Klentaq and KF are higher fidelity enzymes, it is probable that they more effectively destabilize the mismatched ternary complex to the extent that no fluorescence change is observable for mismatch binding. This is comparable to the aforementioned case where Pol β demonstrates significantly reduced fluorescence change amplitude in stopped-flow and steady-state experiments compared to the lower fidelity I260Q variant. Paralleling the differences between WT Pol β and I260Q, the differences between high-fidelity Klentaq and KF and lower fidelity Pol β further emphasize the correlation between fidelity and mismatch destabilization.

8.10.5 Computational Studies

8.10.5.1 Molecular Dynamics Simulations

Kinetic data provide mechanistic details of catalysis and lend insight into structural changes occurring for an enzyme during catalysis. Complementarily, crystal and solution structures provide reliable, yet static, pictures of reaction systems during different stages of catalysis. Importantly, modeling and simulation methods bridge the remaining gaps in functional and structural experimental data by providing further information required for a detailed understanding of local and global motions involved along a reaction pathway. In addition to complementing information already obtained from experimental data, modeling studies incite potentially testable experiments regarding enzyme mechanism, and also provide insight into questions that may be experimentally nontestable. In spite of their usefulness in approaching a varied range of problems, molecular mechanics (MM)-based methods have inherent shortcomings because of the use of 'crude' approximations and imperfect force fields, as well as dependence on initial models. As a result, MD simulations of a single DNA polymerase, which employ initial models derived from structures with only minor active-site differences, can produce ambiguous or even conflicting results. However, with the availability of more refined polymerase structures, including structures with well-defined water molecules and catalytic metal ions, the information extracted by MD simulations is continually improving.

MD simulations of the Pol β•DNA system with and without dNTP substrates have been used to delineate the microscopic motions involved in the formation of the catalytic ternary complex. The conformational closing of the N-subdomain upon dNTP binding is accompanied by several functionally relevant movements in key Pol β active-site residues, including the rotation of Asp192 to coordinate with the catalytic Mg^{2+}, rotation of Arg258 to interact with Tyr296, and base-flipping of Phe272 to prevent interaction between Arg258 and Asp192 (Figure 18).[184] The order of events and the intermediate states in the conformational closing of Pol β have been further investigated using transition path sampling[159] and stochastic path approaches.[185] These studies show that the sequenced order of events during the N-subdomain closing event is as follows: partial N-subdomain closing, flip of Asp192, partial rotation of Arg258, and completion of N-subdomain closure, flip of Phe272, followed by rearrangement of catalytic region and stabilization of Arg258 in the fully rotated state. The computed conformational landscape shows that the cascade of events along this pathway is highly cooperative. For example, the open ternary complex undergoes partial N-subdomain closing, with a concomitant change in the puckering of the sugar of the incoming dNTP which facilitates base pairing with the templating base. This motion is also coupled with the additional motions involving the incoming dNTP, templating base, and Tyr271 residue to achieve Watson–Crick base pairing. Similarly, the flip of Asp192 is accompanied by the breakage of the salt-bridge between Asp192 and Arg258 residues (Figure 18). In addition to the cooperative motion of residues and substrates, the position and the coordination of the catalytic Mg^{2+} also undergo subtle but systematic transformations.[159] The computed reaction profile and associated free energy barriers suggest that the partial rotation of the Arg258 residue is rate limiting within the conformational closing step.[159] Further computational analysis of the R258A mutant predicted facilitated N-subdomain reopening after chemistry,[186] which was later corroborated experimentally in stopped-flow fluorescence analyses.[138]

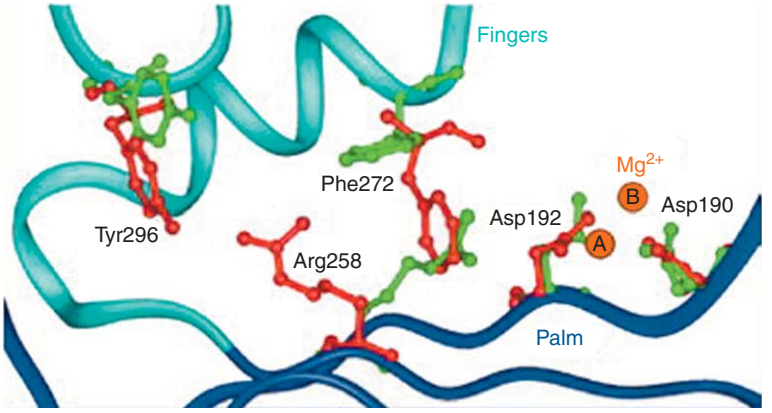

Figure 18 Motion of Arg258 upon N-subdomain (fingers subdomain) closure. Green residues denote the position assumed in the Pol β open state, whereas red residues denote the position assumed in the closed catalytic state. Adapted from L. Yang; W. A. Beard; S. H. Wilson; S. Broyde; T. Schlick, *Biophys. J.* **2004**, *86*, 3392–3408. Permission kindly granted by Tamar Schlick. Copyright 2004 Biophysical Society.

In addition to modeling of the correct dNTP incorporation by Pol β, the influence of the mismatches in the active site of the polymerase has also been investigated using MD simulations. MD simulations indicate that mismatched base pairs at the primer terminus of DNA influence the closing motion of the α-helix N of the N-subdomain, which in turn hampers conformational closing prior to chemistry.[187] Additionally, in these simulations the terminal mismatch base pairs do not adopt a planar conformation, and the presence of a mismatch is shown to influence the ligand arrangement around the Mg^{2+} ions. Transition path sampling simulations comparing G:C matched incorporation versus G:A mismatched incorporation suggest that the cascade of transition states experienced in Pol β conformational closing during mismatched dNTP incorporation is different from the cascade incurred during matched incorporation, and that the mismatched incorporation reaction exhibits a more transient closed state overall.[188] These simulations also suggest that the rate-limiting step for both matched and mismatched nucleotide incorporation pathways occurs after dNTP-induced conformational closing, but prior to the actual phosphoryl transfer. The nature of this step is thought to entail subtle active-site adjustments, including slow adjustments of critical metal/phosphoryl coordinations in the active site. This concept led to the emergence of the term 'pre-chemistry avenue,' used to denote the scenario following N-subdomain conformational closing in which the aforementioned active-site adjustments are required to facilitate an active-site geometry that is poised to support nucleotidyl transfer.[175] As mentioned earlier, it should be noted in terms of general DNA polymerase mechanism discussion, that these local active-site rearrangements should not mechanistically be considered as kinetically distinct steps, but rather considered as a part of the overall chemical step.

In an effort to estimate the contributions of the nucleotide binding, conformational change, and the chemical step to the overall fidelity of T7 DNA polymerase, empirical valence bond (EVB) and linear response approximation (LRA) approaches have been used to calculate the free energy landscape for correct and incorrect dNTP incorporations.[162] **Figure 19** shows the free energy profile as a function of two coordinates: one corresponds to the dNTP-induced conformational closing, and the other corresponds to the chemical reaction. The energy barrier for the conformational closing, for both correct and incorrect dNTP incorporations, is much lower than that for the chemical step, suggesting that the N-subdomain closing is not the rate-determining step. Furthermore, the energetically preferred pathway for mismatched dNTP incorporation is suggested to occur through a partially open enzyme conformation. EVP-LRA methods were also used to explore the role of conformational changes in the fidelity of Pol β.[189] These studies suggest that, similar to T7 polymerase, Pol β also incorporates correct dNTP through a transition state in the closed conformation, whereas incorrect incorporations are realized through transition states in partially open conformations. Consistent with this proposal, recent studies using small-angle X-ray scattering (SAXS) also indicate that incorrect dNTP incorporations catalyzed by Pol β may proceed through a partially open (or partially closed) ternary complex.[190]

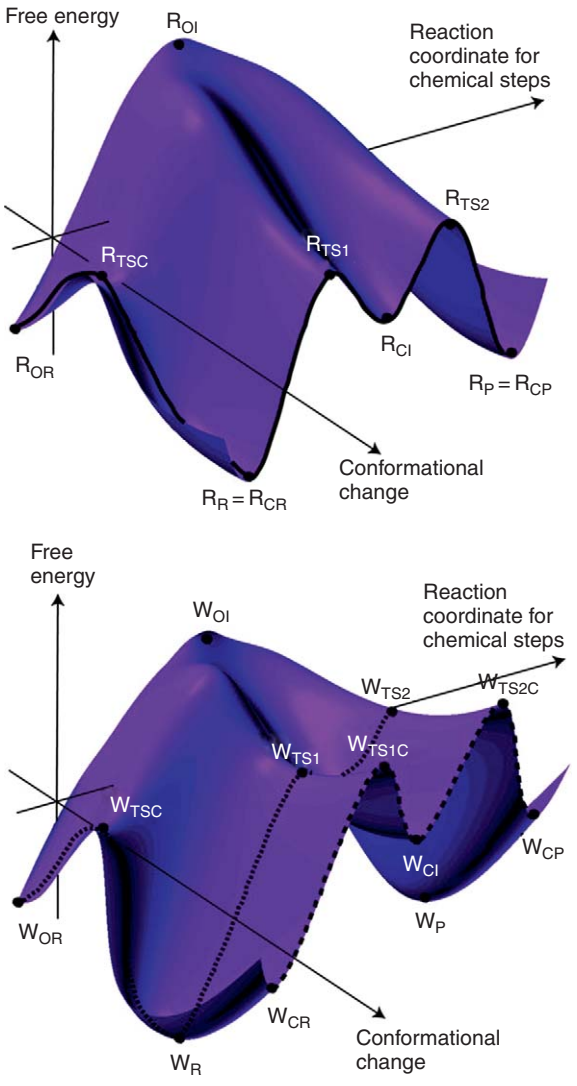

Figure 19 Free energy surfaces for correct (R, top) and incorrect (W, bottom) incorporations by T7 DNA Polymerase. TSC, TS1, and TS2 subscripts refer to transition states for conformational change, O3′-Pα bond formation, and pyrophosphate departure, respectively. W_{TS1C} and W_{TS2C} refer to transition states for mismatched incorporation in a fully closed conformation. Adapted with permission from J. Florian; M. F. Goodman; A. Warshel, *Proc. Natl. Acad. Sci. U.S.A.* **2005**, *102*, 6819–6824. Copyright 2005 National Academy of Sciences.

8.10.5.2 Quantum Mechanical (QM) Studies of the Chemical Step

Although it is important to study the polymerase mechanism in its entirety, it is also interesting to investigate the unfolding of events within the chemical step itself, especially in relation to achievement of the transition state. MM methods do not adequately treat the electronic changes associated with the bond formation/cleavage processes and hence, more sophisticated approaches are required to understand the chemical transformations during catalysis. QM computational studies provide mechanistic details of the catalytic steps at the atomic level and provide useful insights into the origin of mismatch discrimination or fidelity. However, care should be taken while interpreting the results of such analyses because the results show a strong dependence on the initial molecular model.[191]

The mechanism of nucleotidyl transfer during correct dNTP incorporation by DNA polymerases has been investigated by QM methods. The postulated pathway of nucleotidyl transfer includes three critical

microscopic steps. The first step corresponds to the deprotonation of the 3′-OH of the primer. The next step includes nucleophilic attack of the O3′ of the primer on Pα (α-phosphate of dNTP), and is followed by final elimination of the pyrophosphate group.

Several different hypotheses have been proposed for the initial 3′-OH deprotonation event including, direct transfer of the proton to O2α(Pα), transfer of this proton to an active-site aspartate residue, or initial proton transfer to an active-site water molecule, followed by proton migration to an active-site aspartate residue, and finally to pyrophosphate. Starting with an initial model of the active site derived from the Pol β ternary complex structure containing both the catalytic Mg^{2+} ions and the 3′-OH terminal of the primer,[90] QM studies of the chemical step exploring all three hypotheses conclude that the favored catalytic route involves direct proton transfer from O3′ of the primer to the O2α(Pα) of the dNTP through an associative mechanism (**Figure 20**). This leads to the formation of a pentacovalent trigonal bipyramidal Pα center, and is followed by the cleavage of the triphosphate unit and subsequent elimination of the pyrophosphate group.[191] In contrast, computational studies using EVB and QM/MM methods, reveal alternative routes of proton transfer, to either an adjacent Asp residue[192–194] or an active-site water molecule.[195]

Despite several studies focusing on the proton transfer step, there is discrepancy regarding the energetics of individual microscopic steps during nucleotidyl transfer, as QM methods may provide inconsistent results depending on the starting geometry and the computational approach. In the following subsection, we describe the coupling of QM treatment of the active site with empirical simulation of the complete enzyme system.

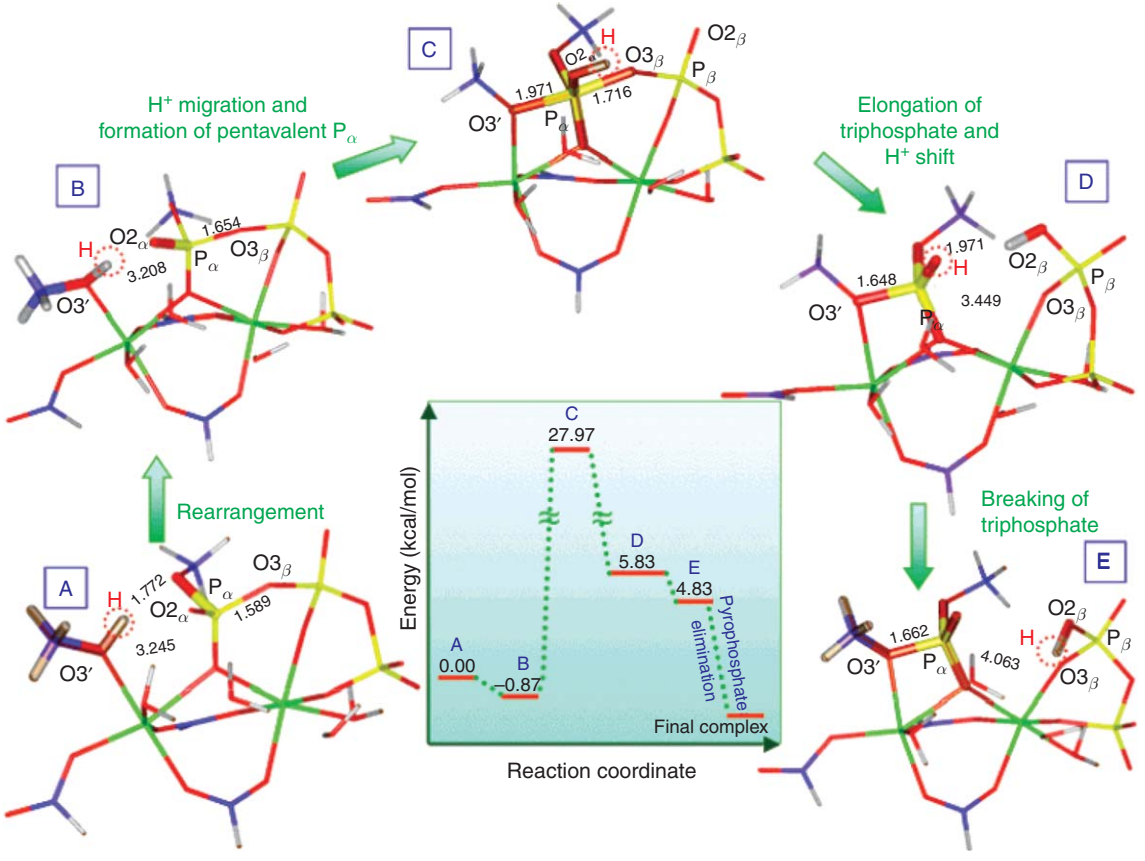

Figure 20 Reaction coordinates for the chemical step of Pol β catalyzed correct nucleotide incorporation and the corresponding structures for each step. Only one of three distinct possible pathways of proton transfer (direct transfer from O3′ to O2α(Pα)) is shown. The atoms are shown as color-coded sticks: Mg (green), P (yellow), O (red), C (blue), and H (gray). Energies are in kcal mol^{-1}. Reproduced with permission from M. D. Bojin; T. Schlick, *J. Phys. Chem. B* **2007**, *111*, 11244–11252. Copyright 2007 American Chemical Society.

8.10.5.3 Mixed QM/MM Studies of the Catalytic Mechanism

Stand-alone QM approaches, by necessity, ignore protein residues and DNA bases not directly involved in catalysis, and additionally do not account for solvent effects. In an attempt to overcome these limitations, several new studies have adopted a mixed quantum and molecular mechanical (QM/MM) approach to study the fully solvated enzyme system. The QM/MM ONIOM approach, has been used to examine the energetic landscape for correct dNTP incorporation by Pol β.[193] This analysis shows that nucleotidyl transfer, following the formation of the ternary complex, is a two-step process in which proton transfer occurs prior to the nucleophilic displacement. The favored route of proton transfer from O3′ to the adjacent Asp256 residue has a lower energy barrier than does the nucleophilic attack (**Figure 21**). The latter is associated with an energy barrier of 14.6 kcal mol^{-1}, comparable to the experimentally derived value of ~16 kcal mol^{-1}. Interestingly, in this study, no stable pentacovalent intermediate was identified.[193] Another study, employing QM/MM dynamics in conjunction with umbrella sampling to estimate free energy of intermediates during the phosphoryl transfer reaction, showed that the dominant pathway of the initial step involves proton transfer from the O3′ to water molecules, followed by proton migration to the Asp256 residue in a series of Grotthuss hopping steps.[195] This pathway of initial proton transfer was also corroborated in another study exploring several different potential mechanisms of the phosphoryl transfer reaction using QM/MM methods.[196] However, this study suggests that the initial deprotonation occurs in conjunction with the nucleophilic attack by O3′ on Pα, with an associated energy barrier of 15.4 kcal mol^{-1}.

Until recently, a detailed understanding of mismatch discrimination by DNA polymerases has been hampered by the lack of structural information on mismatch incorporation by a polymerase. The recent structure of a Pol β mismatch ternary complex[174] has opened the gates for computational analyses of molecular basis of fidelity discrimination. Starting with this structure detailed molecular dynamics (MD) and mixed

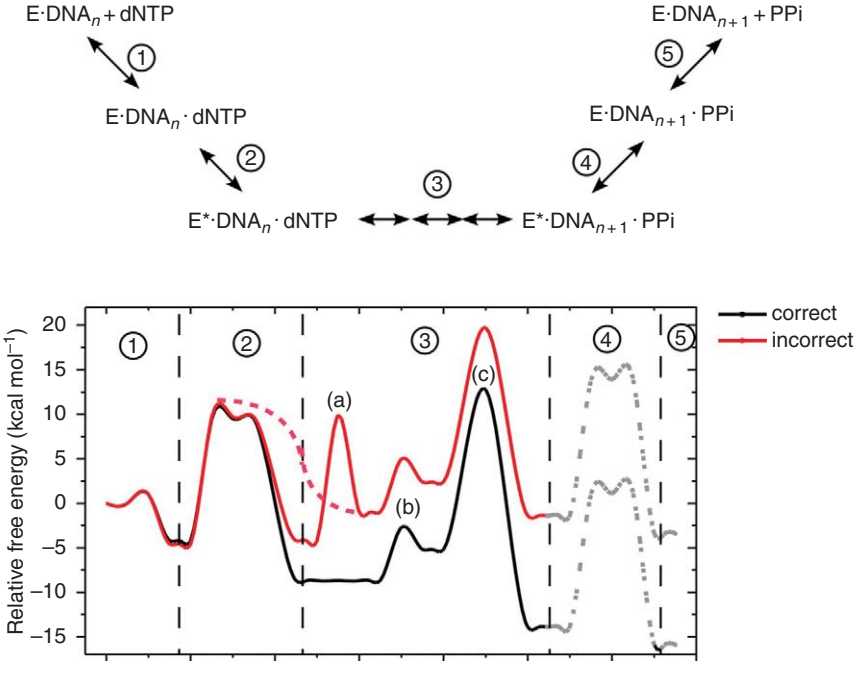

Figure 21 Schematic representation of the free energy profiles for correct (black) and incorrect (red) nucleotide incorporations by Pol β. Reactions follow: initial binding of dNTP (1), open-to-closed conformational change (2), O3′ replacing water in Mg_{cat}^{2+} coordination (3a, for misincorporation only), proton transfer from O3′ to Asp256 (3b), phosphodiester bond formation (3c), closed-to-open conformational change (4), and release of pyrophosphate and Mg ions (5). The dashed lines represent possible transition pathways and barriers. Adapted with permission from P. Lin; V. K. Batra; L. C. Pedersen; W. A. Beard; S. H. Wilson; L. G. Pedersen, *Proc. Natl. Acad. Sci. U.S.A.* **2008**, *105*, 5670–5674. Copyright 2008 by the National Academy of Sciences.

QM/MM computational analyses of the mechanism of G:A mismatch incorporation by Pol β have been performed.[176] The results suggest that for G:A incorporation the most stable conformation of the mismatched ternary complex undergoes additional local structural changes in the active site. These local changes include replacement of an active-site water molecule by O3′ as a ligand for the catalytic Mg^{2+}, resulting in catalytically competent active-site geometry similar to that observed for match G:C incorporation.[193] After this reorganization, the enzyme proceeds to follow the catalytic pathway similar to that for the correct insertion, which involves proton transfer followed by nucleophilic displacement. Similarities in the transition state geometries for matched and mismatched incorporations emphasize the importance of the reaction scaffold formed by triphosphate moiety of dNTP, active site Asp residues, and catalytic Mg^{2+} ions, required for phosphodiester bond formation. The analysis of the energetics of the mismatched versus matched incorporation pathways suggests that the free energy required for destabilization of the ground state to attain a catalytically competent active-site geometry is the major factor contributing to fidelity discrimination (**Figure 21**).[176] This conclusion also correlates well with kinetic evaluations which suggest that the destabilization of the mismatched ternary complex plays an important role in DNA polymerase fidelity.[139]

Over the years, computational methods have elucidated various aspects of the nucleotidyl transfer reaction that complement our knowledge from experimental methods, and provide enhanced insights into the overall mechanism of DNA polymerases. Dynamics simulations have shed light on the subtle and cooperative molecular motions involved during the dNTP-induced conformational closing in Pol β. Calculated energy profiles suggest that this conformational change is not rate limiting in the overall polymerase mechanism. Although there is some ambiguity in literature regarding whether the initial deprotonation of O3′H group is followed by nucleophilic attack by O3′ or whether these processes occur in conjunction, it is generally agreed that pentacovalent transition state formation corresponds to the highest energy barrier within the chemical step and is therefore rate limiting in the overall dNTP incorporation pathway. Quantum mechanical analyses of the catalytic mechanism have shown that the active-site rearrangements prior to nucleotidyl transfer are critical to the overall polymerase mechanism. Both matched and mismatched dNTP incorporation probably follow similar pathways in ultimately achieving catalytically competent active-site geometry prior to nucleotidyl transfer. However, to achieve this geometry, mismatched incorporation may require additional local active-site rearrangements.

Even though this chapter has largely focused on the mechanism of correct dNTP incorporation and the molecular origin of fidelity, the computational approaches described here can also be utilized to study the effects of modified substrates in the active site of polymerases,[197] as well as the effect of interacting proteins on catalysis.[198] Overall, computational methods will continue to be a valuable tool for DNA polymerase mechanism studies. A complete understanding of polymerase mechanism and fidelity will surely be facilitated by future advancements in computational methodology, as well as the availability of new complex structures.

8.10.6 Final Thoughts

Over the past several decades, the collaborative efforts of multiple approaches have brought us to a more comprehensive understanding of the DNA polymerase catalytic mechanism. In attempts to understand the origin of polymerase fidelity, efforts over the past decade encompass extensive pursuits to identify the rate-limiting step during dNTP incorporation, and to provide a structural basis for DNA polymerase selectivity. Most notable progress includes the demonstration that the dNTP-induced subdomain conformational closing is a fast step relative to chemistry. Moreover, large advances in our understanding of mismatch incorporation have been obtained from the crystal structure of a mismatched ternary complex,[174] and results of extensive stopped-flow fluorescence analysis of incorrect dNTP incorporation.[139] The main focus of future research will probably be on detailed structural and mechanistic comparison of mismatched dNTP incorporation with matched dNTP incorporation, in which recent insights into mismatched dNTP incorporation is further investigated with other methods. Additionally, differences among various mispairs also warrant further investigation. Most importantly, in order to fully understand how DNA polymerases control fidelity, the methodological depth of structural and kinetic analyses must be applied to multiple DNA polymerases exhibiting the entire spectrum of fidelity.

Abbreviations

2-AP	2-aminopurine
AP	apurinic/apyridinic
BER	base excision repair
dAMPCPP	2′-deoxyadenosine 5′-α,β-methylenetriphosphate
DNA	deoxyribonucleic acid
dNTP	deoxyribonucleotide triphosphate
dRP	deoxyribosephosphate
DSB	double-strand break
dTMPPCP	2′-deoxythymidine 5′-β,γ-methylenetriphosphate
EVB	empirical valence bond
FRET	fluorescence resonance energy transfer
ICL	interstrand cross-link repair
KF	Klenow fragment
LRA	linear response approximation
MD	molecular dynamics
MM	molecular mechanics
MMR	mismatch repair
NER	nucleotide excision repair
PAD	polymerase-associated domain
Pol	polymerase
QM	quantum mechanics
RNA	ribonucleic acid
SHM	somatic hypermutation
TLS	translesion synthesis
V(D)J	mechanism of genetic recombination
WT	wild type

Nomenclature

Units:

kDa	kilodalton; mass
kcal mol^{-1}	kilocalories per mole; energy
s^{-1}	per second; reaction rate
μmol l^{-1}	micromolar; concentration

Terms:

k_{-1}, k_1, k_{-2}, k_2, k_4	kinetic parameters in polymerase mechanism
K_d	dissociation constant
$K_{d,app}$	apparent dissociation constant
k_{pol}	rate of polymerization

References

1. P. V. Shcherbakova; K. Bebenek; T. A. Kunkel, *Sci. Aging Knowledge Environ.* **2003**, *2003*, RE3.
2. U. Hubscher; G. Maga; S. Spadari, *Annu. Rev. Biochem.* **2002**, *71*, 133–163.
3. Y. I. Pavlov; P. V. Shcherbakova; I. B. Rogozin, *Int. Rev. Cytol.* **2006**, *255*, 41–132.
4. S. D. McCulloch; T. A. Kunkel, *Cell Res.* **2008**, *18*, 148–161.
5. T. A. Kunkel, *Cancer Cell* **2003**, *3*, 105–110.
6. D. Starcevic; S. Dalal; J. B. Sweasy, *Cell Cycle* **2004**, *3*, 998–1001.
7. M. Raszka; N. O. Kaplan, *Proc. Natl. Acad. Sci. U.S.A.* **1972**, *69*, 2025–2029.
8. F. Aboul-ela; D. Koh; I. Tinoco; F. H. Martin, *Nucleic Acids Res.* **1985**, *13*, 4811.
9. L. A. Loeb; T. A. Kunkel, *Annu. Rev. Biochem.* **1982**, *51*, 429–457.
10. J. Ahn; V. S. Kraynov; X. Zhong; B. G. Werneburg; M. D. Tsai, *Biochem. J.* **1998**, *831*, 79–87.
11. J. Ahn; B. G. Werneburg; M. D. Tsai, *Biochemistry* **1997**, *36*, 1100–1107.
12. T. A. Kunkel, *J. Biol. Chem.* **2004**, *279*, 16895–16898.
13. T. A. Kunkel; K. Bebenek, *Annu. Rev. Biochem.* **2000**, *69*, 497–529.
14. M. J. Bessman; A. Kornberg; I. R. Lehman; E. S. Simms, *Biochim. Biophys. Acta* **1956**, *21*, 197–198.
15. I. R. Lehman; M. J. Bessman; E. S. Simms; A. Kornberg, *J. Biol. Chem.* **1958**, *233*, 163–170.
16. M. Delarue; O. Poch; N. Tordo; D. Moras; P. Argos, *Protein Eng.* **1990**, *3*, 461–467.
17. D. K. Braithwaite; J. Ito, *Nucleic Acids Res.* **1993**, *21*, 787–802.
18. J. Ito; D. K. Braithwaite, *Nucleic Acids Res.* **1991**, *19*, 4045–4057.
19. H. Ohmori; E. C. Friedberg; R. P. Fuchs; M. F. Goodman; F. Hanaoka; D. Hinkle; T. A. Kunkel; C. W. Lawrence; Z. Livneh; T. Nohmi; L. Prakash; S. Prakash; T. Todo; G. C. Walker; Z. Wang; R. Woodgate, *Mol. Cell* **2001**, *8*, 7–8.
20. J. B. Sweasy; J. M. Lauper; K. A. Eckert, *Radiat. Res.* **2006**, *166*, 693–714.
21. A. Kornberg, Ed., *DNA Replication*; W. H. Freeman: San Francisco, 1980.
22. A. Kornberg; T. A. Baker, Eds., *DNA Replication*; W. H. Freeman: New York, 1992.
23. L. S. Kaguni, *Annu. Rev. Biochem.* **2004**, *73*, 293–320.
24. M. A. Graziewicz; M. J. Longley; W. C. Copeland, *Chem. Rev.* **2006**, *106*, 383–405.
25. M. J. Longley; R. Prasad; D. K. Srivastava; S. H. Wilson; W. C. Copeland, *Proc. Natl. Acad. Sci. U.S.A.* **1998**, *95*, 12244–12248.
26. S. W. Graves; A. A. Johnson; K. A. Johnson, *Biochemistry* **1998**, *37*, 6050–6058.
27. K. Takata; T. Shimizu; S. Iwai; R. D. Wood, *J. Biol. Chem.* **2006**, *281*, 23445–23455.
28. M. E. Arana; K. Takata; M. Garcia-Diaz; R. D. Wood; T. A. Kunkel, *DNA Repair* **2007**, *6*, 213–223.
29. M. Seki; R. D. Wood, *DNA Repair* **2008**, *7*, 119–127.
30. M. Seki; F. Marini; R. D. Wood, *Nucleic Acids Res.* **2003**, *31*, 6117–6126.
31. M. Seki; C. Masutani; L. W. Yang; A. Schuffert; S. Iwai; I. Bahar; R. D. Wood, *EMBO J.* **2004**, *23*, 4484–4494.
32. K. Masuda; R. Ouchida; A. Takeuchi; T. Saito; H. Koseki; K. Kawamura; M. Tagawa; T. Tokuhisa; T. Azuma; J. O-Wang, *Proc. Natl. Acad. Sci. U.S.A.* **2005**, *102*, 13986–13991.
33. H. Zan; N. Shima; Z. Xu; A. Al-Qahtani; A. J. Evinger Iii; Y. Zhong; J. C. Schimenti; P. Casali, *EMBO J.* **2005**, *24*, 3757–3769.
34. K. Masuda; R. Ouchida; M. Hikida; M. Nakayama; O. Ohara; T. Kurosaki; J. O-Wang, *DNA Repair* **2006**, *5*, 1384–1391.
35. H. Pospiech; J. E. Syvaoja, *Sci. World J.* **2003**, *3*, 87–104.
36. R. Hindges; U. Hubscher, *Biol. Chem.* **1997**, *378*, 345–362.
37. I. R. Lehman; L. S. Kaguni, *J. Biol. Chem.* **1989**, *264*, 4265–4268.
38. A. Johnson; M. O'Donnell, *Annu. Rev. Biochem.* **2005**, *74*, 283–315.
39. C. W. Lawrence, *Adv. Protein Chem.* **2004**, *69*, 167–203.
40. G. N. Gan; J. P. Wittschieben; B. O. Wittschieben; R. D. Wood, *Cell Res.* **2008**, *18*, 174–183.
41. Z. Kelman; M. O'Donnell, *Annu. Rev. Biochem.* **1995**, *64*, 171–200.
42. M. O'Donnell; D. Jeruzalmi; J. Kuriyan, *Curr. Biol.* **2001**, *11*, R935–R946.
43. I. K. Cann; Y. Ishino, *Genetics* **1999**, *152*, 1249–1267.
44. Y. Kubota; R. A. Nash; A. Klungland; P. Schar; D. E. Barnes; T. Lindahl, *EMBO J.* **1996**, *15*, 6662–6670.
45. I. D. Nicholl; K. Nealon; M. K. Kenny, *Biochemistry* **1997**, *36*, 7557–7566.
46. R. W. Sobol; J. K. Horton; R. Kuhn; H. Gu; R. K. Singhal; R. Prasad; K. Rajewsky; S. H. Wilson, *Nature* **1996**, *379*, 183–186.
47. S. S. Parikh; C. D. Mol; J. A. Tainer, *Structure* **1997**, *5*, 1543–1550.
48. S. H. Wilson, *Mutat. Res.* **1998**, *407*, 203–215.
49. T. Lindahl; R. D. Wood, *Science* **1999**, *286*, 1897–1905.
50. C. E. Piersen; R. Prasad; S. H. Wilson; R. S. Lloyd, *J. Biol. Chem.* **1996**, *271*, 17811–17815.
51. R. Prasad; R. K. Singhal; D. K. Srivastava; J. T. Molina; A. E. Tomkinson; S. H. Wilson, *J. Biol. Chem.* **1996**, *271*, 16000–16007.
52. R. A. Nash; K. W. Caldecott; D. E. Barnes; T. Lindahl, *Biochemistry* **1997**, *36*, 5207–5211.
53. S. Gilfillan; C. Benoist; D. Mathis, *Immunol. Rev.* **1995**, *148*, 201–219.
54. T. Komori; A. Okada; V. Stewart; F. W. Alt, *Science* **1993**, *261*, 1171–1175.
55. S. Gilfillan; A. Dierich; M. Lemeur; C. Benoist; D. Mathis, *Science* **1993**, *261*, 1175–1178.
56. J. D. Fowler; Z. Suo, *Chem. Rev.* **2006**, *106*, 2092–2110.
57. S. A. Nick McElhinny; D. A. Ramsden, *Immunol. Rev.* **2004**, *200*, 156–164.
58. A. F. Moon; M. Garcia-Diaz; V. K. Batra; W. A. Beard; K. Bebenek; T. A. Kunkel; S. H. Wilson; L. C. Pedersen, *DNA Repair* **2007**, *6*, 1709–1725.
59. D. R. Carson; M. F. Christman, *Proc. Natl. Acad. Sci. U.S.A.* **2001**, *98*, 8270–8275.
60. Z. Wang; I. B. Castano; A. De Las Penas; C. Adams; M. F. Christman, *Science* **2000**, *289*, 774–779.
61. M. Oliveros; R. J. Yanez; M. L. Salas; J. Salas; E. Vinuela; L. Blanco, *J. Biol. Chem.* **1997**, *272*, 30899–30910.
62. A. J. Rattray; J. N. Strathern, *Annu. Rev. Genet.* **2003**, *37*, 31–66.
63. S. Prakash; R. E. Johnson; L. Prakash, *Annu. Rev. Biochem.* **2005**, *74*, 317–353.

64. A. R. Lehmann; A. Niimi; T. Ogi; S. Brown; S. Sabbioneda; J. F. Wing; P. L. Kannouche; C. M. Green, *DNA Repair* **2007**, *6*, 891–899.
65. A. R. Lehmann, *Exp. Cell Res.* **2006**, *312*, 2673–2676.
66. A. R. Lehmann, *Mol. Cell* **2006**, *24*, 493–495.
67. P. Kannouche; A. Lehmann, *Meth. Enzymol.* **2006**, *408*, 407–415.
68. S. Prakash; L. Prakash, *Genes Dev.* **2002**, *16*, 1872–1883.
69. T. A. Kunkel; Y. I. Pavlov; K. Bebenek, *DNA Repair* **2003**, *2*, 135–149.
70. A. Vaisman; A. R. Lehmann; R. Woodgate, *Adv. Protein Chem.* **2004**, *69*, 205–228.
71. B. Oberg, *Antiviral Res.* **2006**, *71*, 90–95.
72. H. C. Castro; N. I. Loureiro; M. Pujol-Luz; A. M. Souza; M. G. Albuquerque; D. O. Santos; L. M. Cabral; I. C. Frugulhetti; C. R. Rodrigues, *Curr. Med. Chem.* **2006**, *13*, 313–324.
73. M. Gotte, *Curr. Pharm. Des.* **2006**, *12*, 1867–1877.
74. R. Prasad; W. A. Beard; S. H. Wilson, *J. Biol. Chem.* **1994**, *269*, 18096–18101.
75. Y. Matsumoto; K. Kim, *Science* **1995**, *269*, 699–702.
76. R. Prasad; W. A. Beard; P. R. Strauss; S. H. Wilson, *J. Biol. Chem.* **1998**, *273*, 15263–15270.
77. M. R. Sawaya; H. Pelletier; A. Kumar; S. H. Wilson; J. Kraut, *Science* **1994**, *264*, 1930–1935.
78. M. R. Sawaya; R. Prasad; S. H. Wilson; J. Kraut; H. Pelletier, *Biochemistry* **1997**, *36*, 11205–11215.
79. H. Huang; R. Chopra; G. L. Verdine; S. C. Harrison, *Science* **1998**, *282*, 1669–1675.
80. S. Doublie; S. Tabor; A. M. Long; C. C. Richardson; T. Ellenberger, *Nature* **1998**, *391*, 251–258.
81. D. L. Ollis; P. Brick; R. Hamlin; N. G. Xuong; T. A. Steitz, *Nature* **1985**, *313*, 762–766.
82. T. A. Steitz; S. J. Smerdon; J. Jager; C. M. Joyce, *Science* **1994**, *266*, 2022–2025.
83. W. A. Beard; S. H. Wilson, *Chem. Rev.* **2006**, *106*, 361–382.
84. F. Boudsocq; R. J. Kokoska; B. S. Plosky; A. Vaisman; H. Ling; T. A. Kunkel; W. Yang; R. Woodgate, *J. Biol. Chem.* **2004**, *279*, 32932–32940.
85. J. F. Davies 2nd; R. J. Almassy; Z. Hostomska; R. A. Ferre; Z. Hostomsky, *Cell* **1994**, *76*, 1123–1133.
86. H. Pelletier; M. R. Sawaya; A. Kumar; S. H. Wilson; J. Kraut, *Science* **1994**, *264*, 1891–1903.
87. H. Pelletier; M. R. Sawaya; W. Wolfle; S. H. Wilson; J. Kraut, *Biochemistry* **1996**, *35*, 12742–12761.
88. H. Pelletier; M. R. Sawaya; W. Wolfle; S. H. Wilson; J. Kraut, *Biochemistry* **1996**, *35*, 12762–12777.
89. J. W. Arndt; W. Gong; X. Zhong; A. K. Showalter; J. Liu; C. A. Dunlap; Z. Lin; C. Paxson; M.-D. Tsai; M. K. Chan, *Biochemistry* **2001**, *40*, 5368–5375.
90. V. K. Batra; W. A. Beard; D. D. Shock; J. M. Krahn; L. C. Pedersen; S. H. Wilson, *Structure* **2006**, *14*, 757–766.
91. Y. Li; S. Korolev; G. Waksman, *EMBO J.* **1998**, *17*, 7514–7525.
92. K. A. Johnson, *Annu. Rev. Biochem.* **1993**, *62*, 685–713.
93. S. Doublie; M. R. Sawaya; T. Ellenberger, *Structure* **1999**, *7*, R31–R35.
94. E. T. Kool, *Annu. Rev. Biochem.* **2002**, *71*, 191–219.
95. H. Ling; F. Boudsocq; R. Woodgate; W. Yang, *Cell* **2001**, *107*, 91–102.
96. J. H. Wong; K. A. Fiala; Z. Suo; H. Ling, *J. Mol. Biol.* **2008**, *379*, 317–330.
97. O. Rechkoblit; L. Malinina; Y. Cheng; V. Kuryavyi; S. Broyde; N. E. Geacintov; D. J. Patel, *PLoS Biol.* **2006**, *4*, e11.
98. D. T. Nair; R. E. Johnson; L. Prakash; S. Prakash; A. K. Aggarwal, *Nat. Struct. Mol. Biol.* **2006**, *13*, 619–625.
99. T. A. Steitz, *Curr. Opin. Struct. Biol.* **1993**, *3*, 31–38.
100. T. A. Steitz, *J. Biol. Chem.* **1999**, *274*, 17395–17398.
101. M. E. Dahlberg; S. J. Benkovic, *Biochemistry* **1991**, *30*, 4835–4843.
102. B. T. Eger; S. J. Benkovic, *Biochemistry* **1992**, *31*, 9227–9236.
103. R. D. Kuchta; P. Benkovic; S. J. Benkovic, *Biochemistry* **1988**, *27*, 6716–6725.
104. R. D. Kuchta; V. Mizrahi; P. A. Benkovic; K. A. Johnson; S. J. Benkovic, *Biochemistry* **1987**, *26*, 8410–8417.
105. S. S. Patel; I. Wong; K. A. Johnson, *Biochemistry* **1991**, *30*, 511–525.
106. I. Wong; S. S. Patel; K. A. Johnson, *Biochemistry* **1991**, *30*, 526–537.
107. W. A. Beard; D. D. Shock; B. J. Vande Berg; S. H. Wilson, *J. Biol. Chem.* **2002**, *277*, 47393–47398.
108. W. A. Beard; S. H. Wilson, *Structure* **2003**, *11*, 489–496.
109. W. R. McClure; T. M. Jovin, *J. Biol. Chem.* **1975**, *250*, 4073–4080.
110. K. Tanabe; E. W. Bohn; S. H. Wilson, *Biochemistry* **1979**, *18*, 3401–3406.
111. T. S. F. Wang; D. Korn, *Biochemistry* **1982**, *21*, 1597–1608.
112. W. Yang; R. Woodgate, *Proc. Natl. Acad. Sci. U.S.A.* **2007**, *104*, 15591–15598.
113. S. Kumar; M. Bakhtina; M. D. Tsai, *Biochemistry* **2008**, *47*, 7875–7887.
114. P. M. Burgers; F. Eckstein, *J. Biol. Chem.* **1979**, *254*, 6889–6893.
115. J. Liu; M. D. Tsai, *Biochemistry* **2001**, *40*, 9014–9022.
116. D. Herschlag; J. A. Piccirilli; T. R. Cech, *Biochemistry* **1991**, *30*, 4844–4854.
117. B. G. Werneburg; J. Ahn; X. Zhong; R. J. Hondal; V. S. Kraynov; M. D. Tsai, *Biochemistry* **1996**, *35*, 7041–7050.
118. C. A. Sucato; T. G. Upton; B. A. Kashemirov; V. K. Batra; V. Martinek; Y. Xiang; W. A. Beard; L. C. Pedersen; S. H. Wilson; C. E. McKenna; J. Florian; A. Warshel; M. F. Goodman, *Biochemistry* **2007**, *46*, 461–471.
119. C. A. Sucato; T. G. Upton; B. A. Kashemirov; J. Osuna; K. Oertell; W. A. Beard; S. H. Wilson; J. Florian; A. Warshel; C. E. McKenna; M. F. Goodman, *Biochemistry* **2008**, *47*, 870–879.
120. K. H. Jung; A. Marx, *Cell. Mol. Life Sci.* **2005**, *62*, 2080–2091.
121. J. Beckman; K. Kincaid; M. Hocek; T. Spratt; J. Engels; R. Cosstick; R. D. Kuchta, *Biochemistry* **2007**, *46*, 448–460.
122. A. T. Krueger; E. T. Kool, *Curr. Opin. Chem. Biol.* **2007**, *11*, 588–594.
123. J. C. Morales; E. T. Kool, *J. Am. Chem. Soc.* **2000**, *122*, 1001–1007.
124. S. Moran; R. X. F. Ren; S. Rumney; E. T. Kool, *J. Am. Chem. Soc.* **1997**, *119*, 2056–2057.
125. O. Potapova; C. Chan; A. M. DeLucia; S. A. Helquist; E. T. Kool; N. D. Grindley; C. M. Joyce, *Biochemistry* **2006**, *45*, 890–898.
126. T. W. Kim; J. C. Delaney; J. M. Essigmann; E. T. Kool, *Proc. Natl. Acad. Sci. U.S.A.* **2005**, *102*, 15803–15808.

127. H. R. Lee; S. A. Helquist; E. T. Kool; K. A. Johnson, *J. Biol. Chem.* **2008**, *283*, 14402–14410.
128. M. Garcia-Diaz; K. Bebenek; J. M. Krahn; T. A. Kunkel; L. C. Pedersen, *Nat. Struct. Mol. Biol.* **2005**, *12*, 97–98.
129. A. F. Moon; M. Garcia-Diaz; K. Bebenek; B. J. Davis; X. Zhong; D. A. Ramsden; T. A. Kunkel; L. C. Pedersen, *Nat. Struct. Mol. Biol.* **2007**, *14*, 45–53.
130. J. F. Ruiz; R. Juarez; M. Garcia-Diaz; G. Terrados; A. J. Picher; S. Gonzalez-Barrera; A. R. Fernandez de Henestrosa; L. Blanco, *Nucleic Acids Res.* **2003**, *31*, 4441–4449.
131. M. Astatke; K. Ng; N. D. Grindley; C. M. Joyce, *Proc. Natl. Acad. Sci. U.S.A.* **1998**, *95*, 3402–3407.
132. A. Bonnin; J. M. Lazaro; L. Blanco; M. Salas, *J. Mol. Biol.* **1999**, *290*, 241–251.
133. G. Gao; M. Orlova; M. M. Georgiadis; W. A. Hendrickson; S. P. Goff, *Proc. Natl. Acad. Sci. U.S.A.* **1997**, *94*, 407–411.
134. C. M. Joyce, *Proc. Natl. Acad. Sci. U.S.A.* **1997**, *94*, 1619–1622.
135. P. H. Patel; L. A. Loeb, *J. Biol. Chem.* **2000**, *275*, 40266–40272.
136. T. Date; S. Yamamoto; K. Tanihara; Y. Nishimoto; A. Matsukage, *Biochemistry* **1991**, *30*, 5286–5292.
137. K. L. Menge; Z. Hostomsky; B. R. Nodes; G. O. Hudson; S. Rahmati; E. W. Moomaw; R. J. Almassy; Z. Hostomska, *Biochemistry* **1995**, *34*, 15934–15942.
138. M. Bakhtina; M. P. Roettger; S. Kumar; M. D. Tsai, *Biochemistry* **2007**, *46*, 5463–5472.
139. M. P. Roettger; M. Bakhtina; M. D. Tsai, *Biochemistry* **2008**, *47*, 9718–9727.
140. C. A. Dunlap; M. D. Tsai, *Biochemistry* **2002**, *41*, 11226–11235.
141. A. M. DeLucia; N. D. Grindley; C. M. Joyce, *Biochemistry* **2007**, *46*, 10790–10803.
142. V. Purohit; N. D. Grindley; C. M. Joyce, *Biochemistry* **2003**, *42*, 10200–10211.
143. C. Hariharan; L. B. Bloom; S. A. Helquist; E. T. Kool; L. J. Reha-Krantz, *Biochemistry* **2006**, *45*, 2836–2844.
144. X. Zhong; S. S. Patel; B. G. Werneburg; M. D. Tsai, *Biochemistry* **1997**, *36*, 11891–11900.
145. Y. C. Tsai; K. A. Johnson, *Biochemistry* **2006**, *45*, 9675–9687.
146. C. M. Joyce; O. Potapova; A. M. Delucia; X. Huang; V. P. Basu; N. D. Grindley, *Biochemistry* **2008**, *47*, 6103–6116.
147. P. J. Rothwell; V. Mitaksov; G. Waksman, *Mol. Cell* **2005**, *19*, 345–355.
148. G. Stengel; J. P. Gill; P. Sandin; L. M. Wilhelmsson; B. Albinsson; B. Norden; D. Millar, *Biochemistry* **2007**, *46*, 12289–12297.
149. G. Luo; M. Wang; W. H. Konigsberg; X. S. Xie, *Proc. Natl. Acad. Sci. U.S.A.* **2007**, *104*, 12610–12615.
150. P. J. Rothwell; G. Waksman, *J. Biol. Chem.* **2007**, *282*, 28884–28892.
151. M. Bakhtina; S. Lee; Y. Wang; C. Dunlap; B. Lamarche; M. D. Tsai, *Biochemistry* **2005**, *44*, 5177–5187.
152. E. L. Rachofsky; R. Osman; J. B. Ross, *Biochemistry* **2001**, *40*, 946–956.
153. M. Bakhtina; M. P. Roettger; M. D. Tsai, *Biochemistry* **2009**, *48*, 3197–3208.
154. A. C. Brouwer; J. F. Kirsch, *Biochemistry* **1982**, *21*, 1302–1307.
155. B. Gavish; M. M. Werber, *Biochemistry* **1979**, *18*, 1269–1275.
156. L. C. Kurz; E. Weitkamp; C. Frieden, *Biochemistry* **1987**, *26*, 3027–3032.
157. J. Lew; S. S. Taylor; J. A. Adams, *Biochemistry* **1997**, *36*, 6717–6724.
158. J. W. Beckman; Q. Wang; F. P. Guengerich, *J. Biol. Chem.* **2008**, *283*, 36711–36723.
159. R. Radhakrishnan; T. Schlick, *Proc. Natl. Acad. Sci. U.S.A.* **2004**, *101*, 5970–5975.
160. L. Yang; W. A. Beard; S. H. Wilson; S. Broyde; T. Schlick, *J. Mol. Biol.* **2002**, *317*, 651–671.
161. K. A. Johnson, *J. Biol. Chem.* **2008**, *283*, 26297–26301.
162. J. Florian; M. F. Goodman; A. Warshel, *Proc. Natl. Acad. Sci. U.S.A.* **2005**, *102*, 6819–6824.
163. J. A. Cowan, *Chem. Rev.* **1998**, *98*, 1067–1087.
164. W. W. Cleland, *Meth. Enzymol.* **1982**, *87*, 159–179.
165. X. Zhong; S. S. Patel; M.-D. Tsai, *J. Am. Chem. Soc.* **1998**, *120*, 235–236.
166. A. K. Showalter; B. J. Lamarche; M. Bakhtina; M. I. Su; K. H. Tang; M. D. Tsai, *Chem. Rev.* **2006**, *106*, 340–360.
167. A. K. Showalter; M. D. Tsai, *Biochemistry* **2002**, *41*, 10571–10576.
168. C. M. Joyce; S. J. Benkovic, *Biochemistry* **2004**, *43*, 14317–14324.
169. J. M. Krahn; W. A. Beard; S. H. Wilson, *Structure* **2004**, *12*, 1823–1832.
170. Y. Xiang; P. Oelschlaeger; J. Florian; M. F. Goodman; A. Warshel, *Biochemistry* **2006**, *45*, 7036–7048.
171. S. J. Johnson; L. S. Beese, *Cell* **2004**, *116*, 803–816.
172. J. Trincao; R. E. Johnson; W. T. Wolfle; C. R. Escalante; S. Prakash; L. Prakash; A. K. Aggarwal, *Nat. Struct. Mol. Biol.* **2004**, *11*, 457–462.
173. V. K. Batra; W. A. Beard; D. D. Shock; L. C. Pedersen; S. H. Wilson, *Structure* **2005**, *13*, 1225–1233.
174. V. K. Batra; W. A. Beard; D. D. Shock; L. C. Pedersen; S. H. Wilson, *Mol. Cell* **2008**, *30*, 315–324.
175. R. Radhakrishnan; K. Arora; Y. Wang; W. A. Beard; S. H. Wilson; T. Schlick, *Biochemistry* **2006**, *45*, 15142–15156.
176. P. Lin; V. K. Batra; L. C. Pedersen; W. A. Beard; S. H. Wilson; L. G. Pedersen, *Proc. Natl. Acad. Sci. U.S.A.* **2008**, *105*, 5670–5674.
177. A. K. Showalter; M. D. Tsai, *J. Am. Chem. Soc.* **2001**, *123*, 1776–1777.
178. M. P. Roettger; K. A. Fiala; S. Sompalli; Y. Dong; Z. Suo, *Biochemistry* **2004**, *43*, 13827–13838.
179. W. M. Kati; K. A. Johnson; L. F. Jerva; K. S. Anderson, *J. Biol. Chem.* **1992**, *267*, 25988–25997.
180. K. A. Fiala; W. Abdel-Gawad; Z. Suo, *Biochemistry* **2004**, *43*, 6751–6762.
181. E. Fidalgo da Silva; S. S. Mandal; L. J. Reha-Krantz, *J. Biol. Chem.* **2002**, *277*, 40640–40649.
182. D. Starcevic; S. Dalal; J. Sweasy, *Biochemistry* **2005**, *44*, 3775–3784.
183. D. Starcevic; S. Dalal; J. Jaeger; J. B. Sweasy, *J. Biol. Chem.* **2005**, *280*, 28388–28393.
184. K. Arora; T. Schlick, *Biophys. J.* **2004**, *87*, 3088–3099.
185. K. Arora; T. Schlick, *J. Phys. Chem. Ref. Data* **2005**, *109*, 5358–5367.
186. L. Yang; W. A. Beard; S. H. Wilson; S. Broyde; T. Schlick, *Biophys. J.* **2004**, *86*, 3392–3408.
187. K. Arora; W. A. Beard; S. H. Wilson; T. Schlick, *Biochemistry* **2005**, *44*, 13328–13341.
188. R. Radhakrishnan; T. Schlick, *J. Am. Chem. Soc.* **2005**, *127*, 13245–13252.
189. Y. Xiang; M. F. Goodman; W. A. Beard; S. H. Wilson; A. Warshel, *Proteins* **2008**, *70*, 231–247.
190. K.-H. Tang; M. Niebuhr; C.-S. Tung; H.-c. Chan; C.-C. Chou; M.-D. Tsai, *Nucleic Acids Res.* **2008**, *36*, 2948–2957.

191. M. D. Bojin; T. Schlick, *J. Phys. Chem. B* **2007**, *111*, 11244–11252.
192. J. Florian; M. F. Goodman; A. Warshel, *J. Am. Chem. Soc.* **2003**, *125*, 8163–8177.
193. P. Lin; L. C. Pedersen; V. K. Batra; W. A. Beard; S. H. Wilson; L. G. Pedersen, *Proc. Natl. Acad. Sci. U.S.A.* **2006**, *103*, 13294–13299.
194. R. C. Rittenhouse; W. K. Apostoluk; J. H. Miller; T. P. Straatsma, *Proteins* **2003**, *53*, 667–682.
195. R. Radhakrishnan; T. Schlick, *Biochem. Biophys. Res. Commun.* **2006**, *350*, 521–529.
196. I. L. Alberts; Y. Wang; T. Schlick, *J. Am. Chem. Soc.* **2007**, *129*, 11100–11110.
197. R. Venkatramani; R. Radhakrishnan, *Proteins* **2008**, *71*, 1360–1372.
198. A. Abyzov; A. Uzun; P. R. Strauss; V. A. Ilyin, *PLoS Comput. Biol.* **2008**, *4*, e1000066.

Biographical Sketches

Michelle P. Roettger received her B.S. in biochemistry from Otterbein College, Westerville, Ohio, and her M.S. in biochemistry from The Ohio State University (OSU), Columbus, Ohio. In 2008, she received her Ph.D. in biochemistry from OSU, where she was an NIH Chemistry–Biology Interface Program Fellow. Under the supervision of Ming-Daw Tsai, her dissertation research focused on the catalytic mechanism of DNA polymerase β. Currently, Michelle is working in the pharmaceutical industry under Research & Development.

Marina Bakhtina received a B.S. in molecular biology from Novosibirsk State University, Russia, in 1993. She worked as a research associate for 4 years in the Institute of Molecular Biology (SRC VB 'Vector'), and subsequently earned an M.S. in philosophy from Novosibirsk State University in 1999. Working with Ming-Daw Tsai, she received a Ph.D. in chemistry from OSU in 2006. She is currently a postdoctoral researcher in the Tsai group, where her focus is on the kinetic mechanism of DNA polymerase fidelity.

Sandeep Kumar received his M.S. in chemistry from the Indian Institute of Technology, Kanpur, India, in 2003. He received his Ph.D. from OSU in 2008, where he worked on the catalytic mechanism of DNA polymerases under the supervision of Professor Ming-Daw Tsai. He is currently a post-doctoral researcher with Professors Karin Musier-Forsyth and Christopher Hadad at OSU. His areas of interest include molecular modeling and quantum mechanical investigations of the enzyme mechanisms.

Ming-Daw Tsai received a B.S. degree in chemistry from the National Taiwan University in 1972, a Ph.D. in medicinal chemistry from Purdue University in 1978, and joined the faculty of OSU in 1981. He established the Chemistry–Biology Interface Training Program of OSU in 1996 and served as its director through 2003. He has also directed OSU's Office of Research Campus Chemical Instrument Center for 14 years (1995–2007). In 2008 Tsai led the Institute of Biological Chemistry of Academia Sinica, Taiwan as a director. Tsai has published over 220 articles in chemical and biological journals. His honors include an Alfred P. Sloan Fellowship (1983–85), the Camille and Henry Dreyfus Teacher–Scholar Award (1985–90), the Distinguished Scholar Award of OSU (1992), an Elected Fellow of the American Association for the Advancement of Science (1992), the Kimberly Professor of Chemistry at OSU (2003–07), and Distinguished Alumnus Award (Purdue College of Pharmacy). He also serves on the editorial advisory board of *Biochemistry*. His research interests include mechanistic enzymology and structure–function relationship of proteins in DNA damage response signaling and cancer, particularly ankyrin repeat proteins and FHA domains.